Molecular Cell

Article

RelA-SpoT Homolog toxins pyrophosphorylate the CCA end of tRNA to inhibit protein synthesis

Graphical abstract

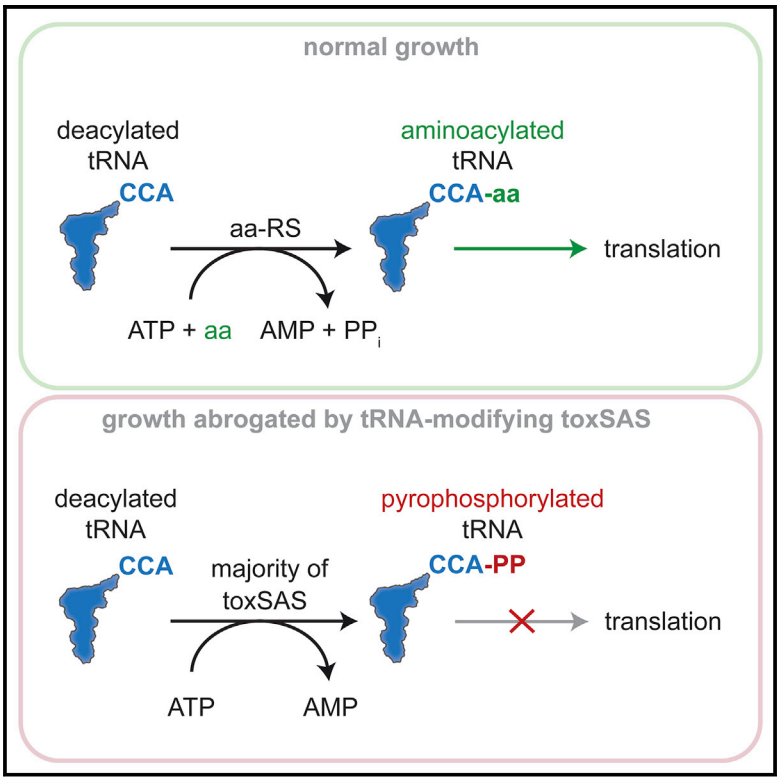

Highlights

- Several families of toxSAS RSH toxins specifically inhibit protein synthesis
- Translation-inhibiting toxSASs transfer pyrophosphate from ATP to the tRNA 3′ CCA
- 3′ CCA pyrophosphorylation abrogates tRNA aminoacylation
- Some SAH RSH enzymes can reverse the pyrophosphorylation of tRNA

Authors

Tatsuaki Kurata,
Tetiana Brodiazhenko,
Sofia Raquel Alves Oliveira, ...,
Abel Garcia-Pino,
Gemma Catherine Atkinson,
Vasili Hauryliuk

Correspondence

tatsuaki.kurata@med.lu.se (T.K.),
gemma.atkinson@med.lu.se (G.C.A.),
vasili.hauryliuk@med.lu.se (V.H.)

In brief

The RelA-SpoT Homolog (RSH) protein family contains both housekeeping stress-response enzymes and toxins of toxin-antitoxin systems (toxSAS). Kurata et al. uncover the mechanism of toxicity used by translation-inhibiting toxSAS. Unlike other RSHs synthetases that produce alarmone nucleotides, most toxSASs are RNA-modifying enzymes that pyrophosphate the tRNA 3′ CCA end.

Kurata et al., 2021, Molecular Cell *81*, 3160–3170
August 5, 2021
https://doi.org/10.1016/j.molcel.2021.06.005

CellPress

CellPress
OPEN ACCESS

Molecular Cell

Article

RelA-SpoT Homolog toxins pyrophosphorylate the CCA end of tRNA to inhibit protein synthesis

Tatsuaki Kurata,[1,*] Tetiana Brodiazhenko,[2] Sofia Raquel Alves Oliveira,[2] Mohammad Roghanian,[3,4] Yuriko Sakaguchi,[5] Kathryn Jane Turnbull,[3,4] Ondřej Bulvas,[6] Hiraku Takada,[7] Hedvig Tamman,[8] Andres Ainelo,[8] Radek Pohl,[6] Dominik Rejman,[6] Tanel Tenson,[2] Tsutomu Suzuki,[5] Abel Garcia-Pino,[8,9] Gemma Catherine Atkinson,[1,*] and Vasili Hauryliuk[1,2,3,10,*]

[1]Department of Experimental Medical Science, Lund University, 221 00 Lund, Sweden
[2]University of Tartu, Institute of Technology, 50411 Tartu, Estonia
[3]Laboratory for Molecular Infection Medicine Sweden (MIMS), Umeå University, 901 87 Umeå, Sweden
[4]Department of Clinical Microbiology, Rigshospitalet, 2200 Copenhagen, Denmark
[5]Department of Chemistry and Biotechnology, Graduate School of Engineering, University of Tokyo, Bunkyo-ku, Tokyo 113-8656, Japan
[6]Institute of Organic Chemistry and Biochemistry, Academy of Sciences of the Czech Republic, v.v.i., Flemingovonam. 2, 166 10 Prague 6, Czech Republic
[7]Faculty of Life Sciences, Kyoto Sangyo University, Kamigamo, Motoyama, Kita-ku, Kyoto 603-8555, Japan
[8]Cellular and Molecular Microbiology (CM2), Faculté des Sciences, Université Libre de Bruxelles (ULB), Campus La Plaine, Building BC, Room 1C4203, Boulevard du Triomphe, 1050 Brussels, Belgium
[9]WELBIO, Avenue Hippocrate 75, 1200 Brussels, Belgium
[10]Lead contact
*Correspondence: tatsuaki.kurata@med.lu.se (T.K.), gemma.atkinson@med.lu.se (G.C.A.), vasili.hauryliuk@med.lu.se (V.H.)
https://doi.org/10.1016/j.molcel.2021.06.005

SUMMARY

RelA-SpoT Homolog (RSH) enzymes control bacterial physiology through synthesis and degradation of the nucleotide alarmone (p)ppGpp. We recently discovered multiple families of small alarmone synthetase (SAS) RSH acting as toxins of toxin-antitoxin (TA) modules, with the FaRel subfamily of toxSAS abrogating bacterial growth by producing an analog of (p)ppGpp, (pp)pApp. Here we probe the mechanism of growth arrest used by four experimentally unexplored subfamilies of toxSAS: FaRel2, PhRel, PhRel2, and CapRel. Surprisingly, all these toxins specifically inhibit protein synthesis. To do so, they transfer a pyrophosphate moiety from ATP to the tRNA 3′ CCA. The modification inhibits both tRNA aminoacylation and the sensing of cellular amino acid starvation by the ribosome-associated RSH RelA. Conversely, we show that some small alarmone hydrolase (SAH) RSH enzymes can reverse the pyrophosphorylation of tRNA to counter the growth inhibition by toxSAS. Collectively, we establish RSHs as RNA-modifying enzymes.

INTRODUCTION

Toxin-antitoxin (TA) systems are a class of highly diverse and widespread small operons found in bacterial, archaeal, and bacteriophage genomes (Fraikin et al., 2020; Harms et al., 2018). TAs have a broad range of functions, including bacterial defense against bacteriophages, phage competition for infection of bacteria, and stabilization of transposons, plasmids, and bacterial genomes, all of which rely on the highly potent toxicity of the protein toxin controlled by the protein- or RNA-based antitoxin (Blower et al., 2009; Fiedoruk et al., 2015; Guegler and Laub, 2021; Jaffé et al., 1985; Lima-Mendez et al., 2020; Song and Wood, 2020). Many TA toxins are closely evolutionary related to housekeeping enzymes, suggesting a "breakaway" evolutionary path on which a generally harmless enzyme evolves a toxic function that requires tight control by the antitoxin (Burckhardt and Escalante-Semerena, 2020; Garcia-Pino et al., 2014; Jimmy et al., 2020; Koonin and Makarova, 2019; Senissar et al., 2017).

The RelA-SpoT Homolog (RSH) protein family of housekeeping stress-response enzymes was only recently recognized to also contain TA toxins (Jimmy et al., 2020). The function of housekeeping RSHs is to control the cellular levels of alarmone nucleotides ppGpp (guanosine-3′,5′-bisdiphosphate) and pppGpp (guanosine-5′-triphosphate-3′-diphosphate), collectively referred to as (p)ppGpp, with the alarmones, in turn, regulating metabolism, virulence, and growth rate, as well as playing an important role in antibiotic and stress tolerance (Gaca et al., 2015; Hauryliuk et al., 2015; Irving et al., 2021; Liu et al., 2015; Zhu et al., 2019). RSH family members can both synthesize (p)ppGpp by transferring the pyrophosphate group of ATP to the 3′ position of either GDP or GTP and convert it back to GDP/GTP through removal of the 3′ pyrophosphate (Atkinson et al., 2011; Cashel and Gallant, 1969). RSHs can be classified into long multi-domain RSHs, with the archetypical representatives being *Escherichia coli* enzymes RelA (Haseltine and Block, 1973) and SpoT (Xiao et al.,

1991), and short single-domain RSHs (Atkinson et al., 2011). The latter are highly diverse and can be subdivided into small alarmone synthetases (SASs; 30 distinct subfamilies, with several representatives characterized experimentally, including *Staphylococcus aureus* RelP [Geiger et al., 2014; Manav et al., 2018] and *Bacillus subtilis* RelQ [Nanamiya et al., 2008; Steinchen et al., 2015]) and small alarmone hydrolases (SAHs; 11 subfamilies) (Jimmy et al., 2020).

Several recent discoveries have sparked interest in how non-(p)ppGpp RSH-mediated chemical catalysis can be weaponized by bacteria for potent growth inhibition. Highly toxic SAS RSH enzymes that are injected by secretion systems (Ahmad et al., 2019) or constitute the toxic components (toxSAS) of TA modules (Jimmy et al., 2020) were found to produce a structural analog of (p)ppGpp—pApp, ppApp, and pppApp—collectively referred to as (pp)pApp (Figure S1). By abrogating *de novo* purine synthesis through orthosteric inhibition of PurF (Ahmad et al., 2019), (pp)pApp inhibits translation, transcription, and replication (Jimmy et al., 2020). SAHs have also been shown to catalyze unexpected non-alarmone reactions; while no (p)ppGpp synthetases are encoded in mammalian genomes, human MESH1 was identified in 2010 as an efficient (p)ppGpp hydrolase (Sun et al., 2010). A decade later, compelling evidence was presented that human MESH1 is a NADPH phosphatase (Ding et al., 2020). Combined with the dramatic evolutionary diversity of this largely experimentally unexplored protein family (Atkinson et al., 2011; Jimmy et al., 2020), these discoveries demonstrate that RSH-mediated catalysis is versatile and that the biological functions of RSH enzymes are clearly not limited to (p)ppGpp metabolism.

We have recently experimentally validated representatives of five toxSAS subfamilies as bona fide TA effectors: *Cellulomonas marina* FaRel, *Bacillus subtilis* la1a PhRel2, *Coprobacillus* sp. D7 FaRel2, *Mycobacterium* phage Phrann PhRel (Gp29), and *Mycobacterium tuberculosis* AB308 CapRel (Jimmy et al., 2020). Out of these, only the (pp)pApp-producing *C. marina* FaRel was previously functionally characterized. In this study we uncover a surprising non-alarmone pyrophosphorylation reaction catalyzed by previously unexplored FaRel2, PhRel2, PhRel, and CapRel enzymes and shed light on how the toxicity of non-alarmone toxSASs can be counteracted through the hydrolytic activity of SAHs.

RESULTS

Representatives of FaRel2, PhRel, PhRel2, and CapRel toxSAS subfamilies specifically inhibit protein synthesis

Although the mechanism of toxicity used by PhRel, PhRel2, FaRel2, and CapRel toxSAS subfamilies is as yet uncharacterized, we initially assumed that these toxSASs, just as *C. marina* FaRel TA toxin (Jimmy et al., 2020) and the Tas1 toxic RSH effector of *Pseudomonas aeruginosa* Type VI secretion system (Ahmad et al., 2019), inhibit bacterial growth by producing (pp)pApp. Surprisingly, when we analyzed the nucleotide pools of growth-arrested *E. coli* expressing *B. subtilis* la1a PhRel2, we detected no accumulation of (pp)pApp (Figure 1A). At the same time, we robustly detected (pp)pApp upon expression of FaRel (Figure S1E; the synthesis of (pp)pApp standards is described in Figure S2). Similarly, we did not detect (pp)pApp upon expression of *Coprobacillus* sp. D7 FaRel2 either (Figure S1H). These results suggested that toxSASs might not universally act via production of (pp)pApp, and therefore, multiple toxSAS subfamilies could have a mechanism of toxicity distinct from that of FaRel and Tas1.

We used metabolic labeling to uncover the effects of as yet uncharacterized toxSASs on translation (by following incorporation of ^{35}S-methionine in proteins), transcription (incorporation of ^{3}H-uridine in RNA), and replication (incorporation of ^{3}H-thymidine in DNA). In stark contrast to FaRel (Jimmy et al., 2020) and Tas1 (Ahmad et al., 2019), which both inhibit all the three processes (Figure S3A), representatives of all four unexplored toxSAS subfamilies specifically inhibited translation. The strongest inhibition was observed for *B. subtilis* la1a PhRel2 and *Coprobacillus* sp. D7 FaRel2 (Figures 1B and 1C), while *M. tuberculosis* AB308 CapRel and *Mycobacterium* phage Phrann superinfection immunity protein PhRel (Gp29) (Dedrick et al., 2017) had a weaker but still specific effect on protein synthesis (Figures S3B and S3C). Interestingly, upon induction of FaRel2, ^{3}H-uridine incorporation increased. This is likely due to abrogation of ATP consumption upon cessation of translation, resulting in increased transcription; earlier we observed a similar effect upon specific inhibition of translation by the antibiotic kanamycin (Jimmy et al., 2020). Furthermore, we observed pronounced stabilization of the polysomal fraction upon expression of *Coprobacillus* sp. D7 FaRel2 (Figure S3D), similar to that observed when translation elongation is stalled by antibiotics (Ennis, 1972). Collectively, our results suggested that specific inhibition of translation is a common mode of toxSAS toxicity, with the FaRel toxSAS subfamily deviating from this common modus operandi.

We next tested whether inhibition of translation by toxSASs is mediated by a direct mechanism using production of dihydrofolate reductase (DHFR) in a reconstituted cell-free protein synthesis system from *E. coli* components (PURE) (Shimizu et al., 2001) as a readout of toxSAS activity. Although purification of toxSAS enzymes is exceedingly challenging (Jimmy et al., 2020), we succeeded in purifying enzymatically competent C-terminally $FLAG_3$-tagged *Coprobacillus* sp. D7 FaRel2 toxin through α-$FLAG_3$ immunoprecipitation (Figure S4). As we have shown earlier, the $FLAG_3$ tag does not interfere with the toxicity of FaRel2 or the ability of the antitoxin to counteract the protein (Jimmy et al., 2020). As a specificity control, we used catalytically compromised FaRel2 variants Y128A (predicted to disrupt the stacking interaction with the pyrophosphate acceptor substrate; Steinchen et al., 2018) and D90G (predicted to compromise the coordination of the Mg^{2+} ion; Steinchen et al., 2015). Both of the substituted residues are highly conserved among SAS RSH enzymes (Figure S5A), and mutant variants are non-toxic when expressed in *E. coli* (Figure 1D). The addition of wild-type, but not D90G or Y128A, FaRel2 to the PURE system abrogated DHFR production (Figure 1E; Figure S6A). The addition of the ATfaRel2 antitoxin, which acts though sequestering FaRel2 into inactive complex (Jimmy et al., 2020), counteracted the inhibitory effect of FaRel2, although not fully (Figure 1F). We concluded that this toxSAS indeed directly targets the protein synthesis machinery.

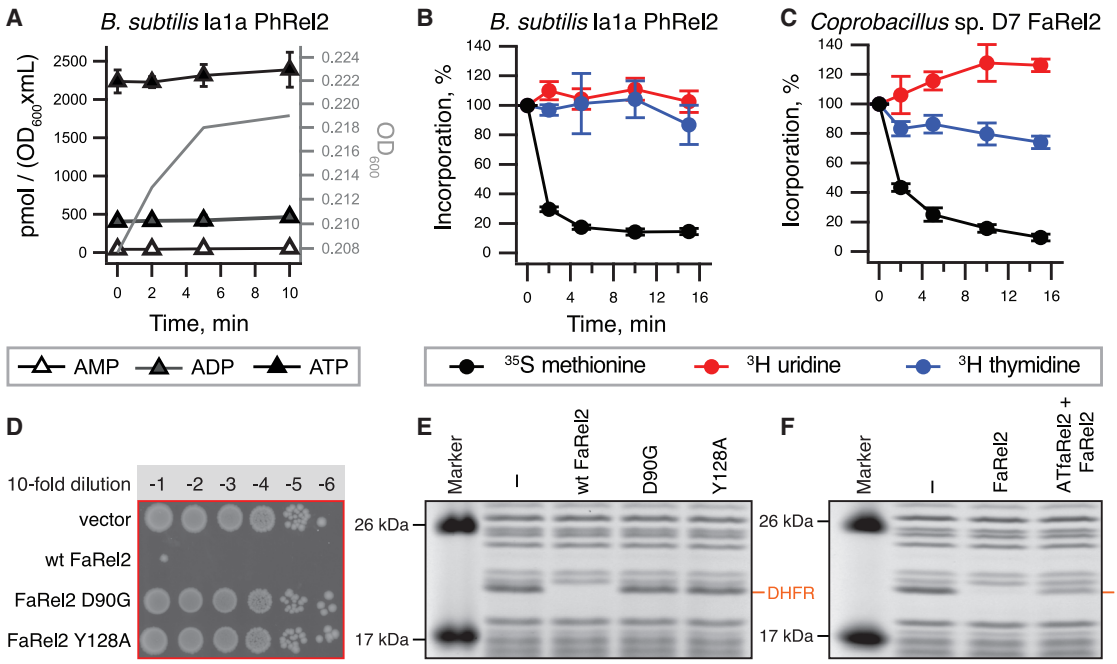

Figure 1. Inhibition of protein synthesis is an evolutionary widespread mechanism of toxSAS-mediated growth arrest

(A) The expression of *B. subtilis* la1a PhRel2 does not perturb the adenosine nucleotide pools, and (pp)pApp is not detectable upon expression of the toxin. Analogous HPLC experiments with *C. marina* FaRel and *Coprobacillus* sp. D7 FaRel2 are presented in Figure S1.

(B and C) Pulse-labeling assays following incorporation of ^{35}S-methionine (black traces), ^{3}H-uridine (red traces), and ^{3}H-thymidine (blue traces). The expression of *B. subtilis* la1a PhRel2 (B) and *Coprobacillus* sp. D7 FaRel2 (C) from the pBAD33-based constructs was induced with 0.2% L-arabinose. Analogous experiments with *P. aeruginosa* Tas1, *Mycobacterium* phage Phrann PhRel (Gp29), and *M. tuberculosis* AB308 CapRel toxSAS are presented in Figure S3.

(D) D90G and Y128A substitutions render FaRel2 non-toxic.

(E and F) Cell-free expression assays. Wild-type but not D90G or Y128A substituted FaRel2 abrogates production of DHFR (E). The addition of the ATfaRel2 antitoxin counteracts the inhibitory effect of FaRel2 (F). ATfaRel2 was combined with FaRel2 prior to adding to the PURE system.

Coprobacillus sp. D7 FaRel2 pyrophosphorylates the 3′ CCA end of tRNA

Inhibition of protein production is a common means of toxicity in TA systems, with the toxic components often acting via modification of tRNA, such as cleavage (used by VapC toxins; Cruz et al., 2015; Winther and Gerdes, 2011), acetylation of the attached amino acid (as seen with GNAT toxins; Cheverton et al., 2016; Jurėnas et al., 2017), or inactivation of the 3′ CCA end through the addition of pyrimidines (used by MenT$_3$; Cai et al., 2020). RSH enzymes have never previously been shown to catalyze synthesis of any other products than hyperphosphorylated nucleotides (pp)pGpp and (pp)pApp. However, one could imagine that the pyrophosphate group of the ATP donor could be transferred onto the ribose position of the 3′ terminal adenosine of tRNA instead of the corresponding 3′ ribose position of the ATP/ADP substrate used by Tas1/FaRel to produce (pp)pApp. As the availability of this 3′ hydroxyl group is essential for tRNA aminoacylation (Weinger and Strobel, 2006), the modification would efficiently inhibit protein synthesis.

We tested this hypothesis using deacylated *E. coli* tRNA as a substrate and γ-^{32}P ATP as a donor of the radioactively labeled pyrophosphate moiety. In the presence of γ-^{32}P ATP, FaRel2 efficiently radiolabels both initiator tRNA$_i^{fMet}$ (Figures 2A and 2B) and elongator tRNA^{Phe} (Figure 2B). To test the generality of toxSAS-mediated translation inhibition via tRNA modification, we purified and tested *B. subtilis* la1a PhRel2. Similarly to *Coprobacillus* FaRel2, PhRel2 efficiently abrogates protein synthesis in the PURE system (Figure 2C), and γ-^{32}P-labels both tRNA$_i^{fMet}$ and tRNA^{Phe} (Figure 2D).

To uncover the nature of the modification, we next characterized the 3′ terminal tRNA modification installed by FaRel2 by capillary liquid chromatography (LC)/nano electrospray ionization mass spectrometry (ESI-MS) analysis of FaRel2-treated *E. coli* tRNA^{Phe} digested by RNase T$_1$ (Figures 2E and 2F; Figure S7). Analysis of the untreated control RNA^{Phe} fragments was used to assign the nature of RNase T$_1$-digested fragments: internal fragments have 5′ hydroxyl (5′OH) and 3′ phosphate (3′P) groups, whereas only the 3′ terminal CACCA-OH fragment has both 5′ and 3′ hydroxyl groups to give unique molecular mass (Figure 2E; Figures S7A and S7C). The CACCA-OH fragment was further probed by higher energy collisional dissociation (HCD), and the sequence was unequivocally confirmed by assignment of its product ions (Figures S7D and S7G). In the FaRel2-treated sample, the abundance of the 3′ terminal CACCA-OH fragment is dramatically decreased (to 4%, relative to the minus FaRel2 sample), and we detected molecular mass corresponding to the RNA fragments bearing pyrophosphate (CACCA-PP, 74%) and cyclic phosphate (CACCA>P, 22%) (Figure 2F; Figures S7B and S7C). The HCD analyses confirmed that the pyrophosphate and cyclic phosphate both occur at

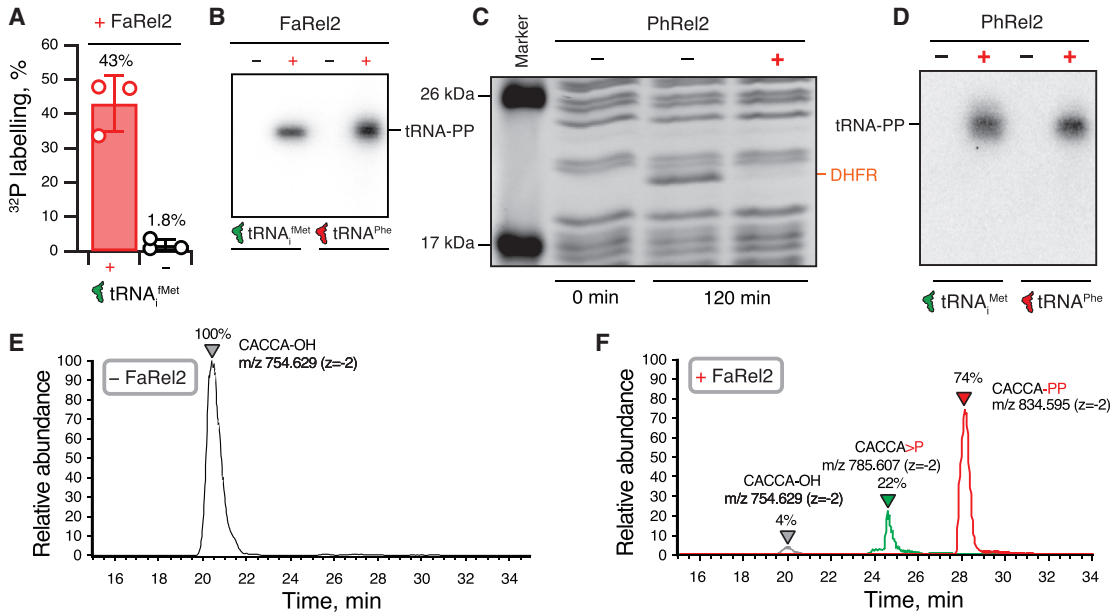

Figure 2. *Coprobacillus* sp. D7 FaRel2 pyrophosphorylates the tRNA 3′ CCA end

(A and B) A reconstituted ^{32}P transfer reaction using 50 nM FaRel2, 100 μM γ^{32}P-ATP, and either 5 μM tRNA$_i^{fMet}$ or 5 μM tRNA^{Phe} as a substrate.

(C) Addition of 100 nM *B. subtilis* Ia1a PhRel2-FLAG$_3$ abrogates production of DHFR in cell-free expression assays.

(D) A reconstituted ^{32}P transfer reaction using 50 nM PhRel2, 100 μM γ^{32}P-ATP, and either 5 μM tRNA$_i^{fMet}$ or 5 μM tRNA^{Phe} as a substrate.

(E and F) Mass spectrometric analysis of FaRel2-modified tRNA^{Phe}. Extracted-ion chromatograms show the deprotonated negative ions of the 3′ terminal fragments (CACCA) with 3′OH, 3′ cyclic phosphate, and 3′ pyrophosphate for either untreated (E) or FaRel2-treated (F) tRNA^{Phe}. The relative abundance of each fragment is calculated from the peak height.

the 3′ terminus of CACCA (Figures S7E–S7G). We speculate that the cyclic phosphate derivative could have been produced from 3′ pyrophosphorylated tRNA^{Phe} through a nucleophilic attack of 2′OH of the tRNA terminus to the 3′ pyrophosphate, resulting in the release of the terminal phosphate. An analogous cyclic derivative of ppGpp, GDP-2′:3′-cyclic monophosphate, was earlier observed in a crystal structure of the N-terminal domain region of long RSH Rel from *Streptococcus dysgalactiae* subsp. *equisimilis* (Hogg et al., 2004).

tRNA 3′ CCA end pyrophosphorylation by FaRel2 abrogates aminoacylation

The tRNA-modifying activity is lost in catalytically compromised D90G and Y128A FaRel2 variants (Figure 3A) and is specifically counteracted by both the AtFaRel2 type II antitoxin and tRNA aminoacylation (Figures 3B and 3C). The latter result is consistent with FaRel2 pyrophosphorylating the 3′ hydroxyl group of the tRNA terminal adenine residue that acts as an amino acid acceptor. To further probe this experimentally, we tested the effect of tRNA modification by FaRel2 on aminoacylation of tRNA^{Phe}. The aminoacylation reaction was readily abrogated by FaRel2 (Figure 3D) in a strictly ATP-dependent manner (Figure 3E), thus explaining the molecular mechanism of translational arrest by this toxSAS. In principle, the FaRel2-modified pyrophospho-tRNA (tRNA-PP) might not just be incompetent in aminoacylation, but also actively toxic to translation because of, for instance, stable binding to the ribosomal A-site or elongation factor EF-Tu. To test this hypothesis, we first titrated total tRNA in the PURE system and identified the near-saturating tRNA concentration (50 μM) at which, we reasoned, the system would be most sensitive to inhibition (Figure S6B). However, added in concentrations up to 14 μM, tRNA^{Phe}-PP had no effect on DHFR synthesis (Figure S6C), suggesting that although tRNA-PP is translation incompetent, it is not inhibitory to the protein synthesis machinery. Rather, the toxicity likely results from a depletion of chargeable tRNA in the cell.

Next, we assessed the specificity of tRNA modification by FaRel2. Both deacylated initiator tRNA$_i^{fMet}$ and elongator tRNA^{Phe} were labeled with ^{32}P by FaRel2 with similar efficiency (Figure 2B), which suggests that the 3′ CCA could be sufficient for recognition of deacylated tRNA. To test this hypothesis and probe the specificity of the toxSAS for tRNA's 3′ adenine residue, we performed radiolabeling experiments with a set of synthetic 5′-CACCN-3′ RNA pentanucleotides containing both the 3′ A as well as 3′ C, G, and U (Figure 3F). Only one of the four RNA substrates, CACCA, was labeled with ^{32}P, suggesting specificity for 3′ adenine. Notably, efficient labeling required a 10-fold higher concentration of the CACCA than that of tRNA (5 versus 50 μM), suggesting that contacts with the tRNA body are also likely to be important for substrate recognition by FaRel2. Finally, the CACCA DNA oligonucleotide did not serve as a FaRel2 substrate, suggesting a functional importance of the 2′ hydroxyl group of the 3′ adenine (Figure 3F). This result is in good agreement with a recent report demonstrating that (p)ppGpp-synthesizing RSH enzymes cannot catalyze the transfer of the

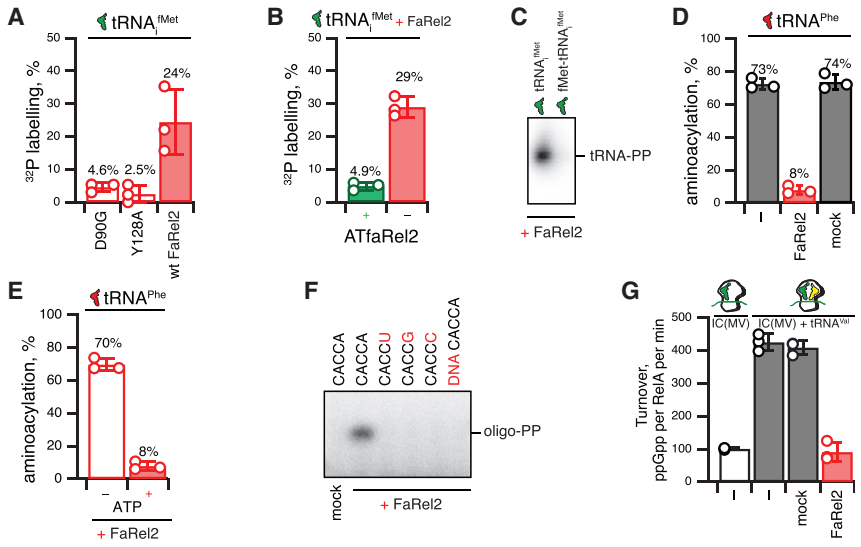

Figure 3. tRNA 3′ CCA end pyrophosphorylation abrogates aminoacylation and the sensing of amino acid starvation by RelA

(A) Non-toxic D90G and Y128A FaRel2 mutants are compromised in their ability to modify tRNA.

(B) The ATfaRel2 antitoxin counteracts tRNA modification by FaRel2.

(C) Acylated fMet-tRNA$_i^{fMet}$ is refractory to modification by FaRel2.

(D) tRNA^{Phe} modification by FaRel2 inhibits aminoacylation. As specificity controls, the reactions were supplemented either with mock protein preparation from an *E. coli* strain transformed with an empty plasmid vector (mock) or HEPES:Polymix buffer (–).

(E) Inhibition of tRNA^{Phe} aminoacylation by FaRel2 is strictly ATP dependent. After the initial preincubation of tRNA^{Phe} with 50 nM FaRel2 of in the presence and absence of ATP, the reaction was supplemented with 2 μM PheRS and ATP. The 40× excess of PheRS over the toxin was used to in order to give the synthetase a kinetic advantage.

(F) 3′ Adenosine defines the specificity of modification by FaRel2, as tested using a set of model 5′-CACCN-3′ RNA oligonucleotides. RNA oligonucleotides were used at final concentration of 50 μM. 5′-CACCA-3′ DNA does not serve as a substrate for FaRel2.

(G) FaRel2 abrogates the stimulatory effect of deacylated 100 nM *E. coli* deacylated tRNA^{Val} on ppGpp synthesis by *E. coli* RelA in the presence of 100 nM 70S ribosomal initiation complexes, 70S IC(MVF). Error bars represent SDs of the mean. The mock sample was produced by immunoprecipitation using *E. coli* cells transformed with a plasmid vector not expressing FLAG$_3$-tagged FaRel2.

pyrophosphate group of the ATP donor to dGTP instead of the GTP substrate (Patil et al., 2020).

tRNA 3′ CCA end pyrophosphorylation by FaRel2 abrogates ribosome-dependent activation of (p)ppGpp synthesis by amino acid starvation sensor RelA

In Gammaproteobacteria such as *E. coli,* amino acid limitation is sensed by a housekeeping multi-domain RSH enzyme RelA (Atkinson et al., 2011). This ribosome-associated factor inspects the aminoacylation status of the 3′ CCA of the A-site tRNA (Arenz et al., 2016; Brown et al., 2016; Loveland et al., 2016) and, upon detecting deacylated tRNA, synthesizes the (p)ppGpp alarmone (Haseltine and Block, 1973). Although the free 3′ OH moiety of the terminal adenosine residue is essential for full activation of RelA's synthesis activity by tRNA on the ribosome (Sprinzl and Richter, 1976), RelA is still activated by the 70S ribosome, although to a lesser extent if activation by tRNA is compromised by the antibiotics thiostrepton (Kudrin et al., 2017) and tetracycline (Kudrin et al., 2018).

Using a reconstituted *E. coli* biochemical system (Kudrin et al., 2018) we tested the effect of FaRel2 on RelA activation by deacylated tRNA^{Val} of starved ribosomal complexes (Figure 3G). FaRel2 efficiently abrogated activation of RelA by tRNA^{Val}, reducing RelA activity to the levels observed in the presence of 70S initiation complexes lacking the A-site deacylated tRNA^{Val}. Thus, not only does FaRel2 not produce an alarmone, it also could prevent the housekeeping RSH cellular machinery from being activated by starved ribosomes to produce the (p)ppGpp alarmone.

FaRel2 prefers *E. coli* tRNA^{Phe} and tRNA$_i^{Met}$ over *E. coli* tRNA^{Val}

As experiments with the reconstituted *E. coli* stringent response system were performed using *E. coli* tRNA^{Val}, we demonstrated that this tRNA species also can be labeled by FaRel2 with ^{32}P (Figure 4A). Notably, the efficiency was seemingly lower than observed for tRNA$_i^{Met}$ and tRNA^{Phe}, with efficient labeling requiring a 10-fold higher concentration of FaRel2 protein, 500 nM, which indicates a certain degree of tRNA specificity. To probe this further, we next tested modification of tRNA$_i^{Met}$, tRNA^{Phe}, and tRNA^{Val} by low concentrations (25 nM) of FaRel2 (Figure 4B). At these conditions, although the signal from tRNA$_i^{Met}$ and tRNA^{Phe} is clear, we did not detect the signal from tRNA^{Val}, clearly suggesting that not all of the tRNA species are recognized by FaRel2 equally well.

SAH RSH enzymes but not the long RSH Rel can restore tRNA aminoacylation competence of FaRel2-modified tRNA

When co-expressed with *Coprobacillus* FaRel2, human MESH1 and *C. marina* ATfaRel hydrolysis-only SAH enzymes can counteract the growth inhibition caused by the toxSAS, although not fully (Figure 5A) (Jimmy et al., 2020). This detoxification activity suggests that MESH1 and ATfaRel can recycle pyrophosphorylated tRNA back to translation-competent deacylated tRNA.

To probe this conjecture experimentally, we pyrophosphorylated tRNA^{Phe} *Coprobacillus* FaRel2, isolated the modified tRNA, and tested whether the human MESH1, *C. marina* ATfaRel, or cognate *Coprobacillus* ATfaRel2 type II antitoxin (not an SAH) could restore the aminoacylation activity of tRNA^{Phe}-PP (Figure 5B). In excellent agreement with our microbiological results (Jimmy et al., 2020) and consistent with CCA pyrophosphorylation's being the cause of growth arrest by FaRel2, both tested SAH enzymes restore the tRNA^{Phe} aminoacylation. At the same time, the long bifunctional RSH Rel from *B. subtilis* could not restore the aminoacylation activity of tRNA^{Phe}-PP (Figure 5B), which explains why the housekeeping long RSH hydrolases such as SpoT present in *E. coli* fail to counteract the toxicity of

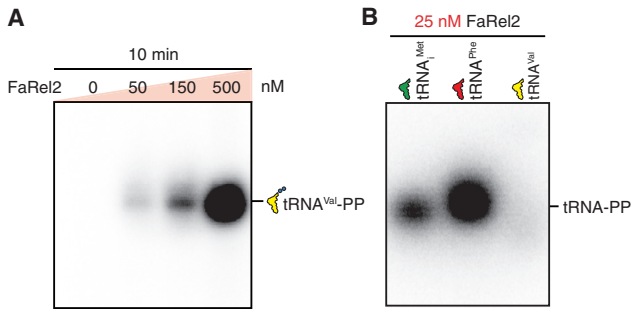

Figure 4. FaRel2 prefers *E. coli* tRNA^{Phe} and tRNA$_i^{Met}$ over *E. coli* tRNA^{Val}

(A) A reconstituted ^{32}P transfer reaction using increasing concentrations of FaRel2 and 5 μM *E. coli* tRNA^{Val} as a substrate.

(B) At low concentrations (25 nM) FaRel2 prefers *E. coli* tRNA^{Phe} and tRNA$_i^{Met}$ substrates over *E. coli* tRNA^{Val}.

FaRel2. Finally, we detected no effect upon the addition of the ATfaRel2 antitoxin, which neutralizes FaRel2 by sequestering the toxSAS into an inactive complex (Jimmy et al., 2020) and therefore is not expected to restore the aminoacylation competence of FaRel2-modified tRNA.

Mapping the tRNA 3′ CCA interaction by FaRel2 through molecular docking and mutagenesis

To gain structural insight into the mechanism of tRNA substrate recognition by FaRel2, we used the Rosetta suite (Song et al., 2013) to model the structure of *Coprobacillus* FaRel2 on the basis of the structures of *S. aureus* housekeeping SAS RelP (Manav et al., 2018) and *B. subtilis* SAS RelQ (Steinchen et al., 2015) (PDB: 6FGK and PDB: 6EWZ, respectively). The model predicted by Rosetta was then used to dock deacylated tRNA^{Phe} into the active site as implemented in the HADDOCK suite (van Zundert et al., 2016). As the only distance restraint in the docking experiment, we used the necessary proximity of FaRel2 Y128 to the CCA-adenine.

The resulting model of the FaRel2-tRNA complex reveals that a cluster of basic residues accommodate the acceptor stem

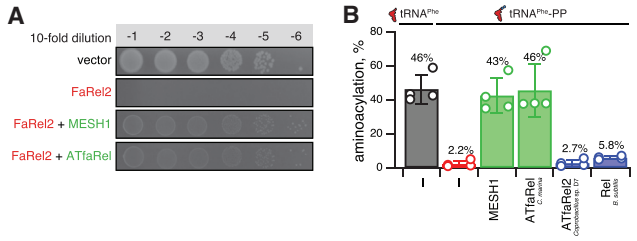

Figure 5. *C. marina* ATfaRel and MESH1 SAH enzymes detoxify FaRel2 through restoration of tRNA aminoacylation

(A) Co-expression of human MESH1 and *C. marina* ATfaRel SAH enzymes counteracts the toxicity of *Coprobacillus* sp. D7 FaRel2 toxSAS. The SAH enzymes and FaRel2 toxSAS were induced and expressed from different plasmids, pMG25 and pMR33 derivatives, respectively.

(B) SAH enzymes MESH1 and ATfaRel but not cognate ATfaRel2 type II antitoxin or long RSH *B. subtilis* Rel restore aminoacylation of tRNA^{Phe} abrogated by FaRel2 by CCA pyrophosphorylation. As specificity controls, the reactions were supplemented with HEPES:Polymix buffer (–).

guiding the CCA end into the active site of the enzyme (Figure 6A). In such an arrangement, the orientation of the 3′-adenosine is reminiscent of the way GDP is coordinated in the active site of housekeeping SAS *S. aureus* RelP (Manav et al., 2018), next to the binding site of ATP, the pyrophosphate donor. Conversely, the analysis of the electrostatic surface profile of RelP and RelQ shows a charge reversal in the same region (Figures S5B and S5C). The presence of a more acidic region in these SASs correlates with a lack of tRNA pyrophosphorylation activity of these enzymes, which would likely be incompatible with tRNA binding.

We probed our molecular model through point mutations in this basic patch, using FaRel2 toxicity as a readout of intact efficient tRNA recognition (Figure 6B). As predicted from our model, Ala substitutions in the basic cluster located toward the N terminus of the toxin that includes K28 and K29 abolished the toxicity of FaRel2. Ala substitutions in the outside rim of the active site (including R114 and Y134), which were predicted to contact the tRNA in our interaction model, also compromise the toxicity of FaRel2. These residues are all outside the active site and would not be involved directly in catalysis, so their effect on toxicity is likely related to tRNA binding. Finally, as a control we confirmed that Ala substitution of basic residues throughout the surface of FaRel2 had no effect on toxicity (Figure 6B).

DISCUSSION

TA toxins belonging to the same protein family can display relaxed specificity toward their targets (Goeders et al., 2013; Harms et al., 2018; Page and Peti, 2016; Schureck et al., 2015; Yamaguchi and Inouye, 2009) or even enzymatically modify clearly distinct classes of substrates (Burckhardt and Escalante-Semerena, 2020; Castro-Roa et al., 2013; Harms et al., 2015; Jurenaite et al., 2013; Jurėnas et al., 2017). A classic example is the GCN5-related N-acetyltransferase (GNAT) TA toxins, a versatile family of enzymes unrelated to RSHs. Although GNAT TA toxins inhibit protein synthesis by acetylating aminoacyl-tRNAs (Cheverton et al., 2016; Jurėnas et al., 2017), the majority of non-toxic GNATs modify small molecules such as polyamines, antibiotics, phospholipids, and amino acids (Burckhardt and Escalante-Semerena, 2020). This substrate specificity spectrum—toxicity mediated via tRNA modification combined with non-toxic modification of small-molecule substrates—is strikingly similar to what we present here for RSH enzymes.

Our results uncover an unexpected enzymatic activity of some toxSAS RSHs to efficiently abrogate translation. We propose the following model of substrate specificity change within the diversity synthetase-competent RSH enzymes (Figure 7). The vast majority of RSH synthetases specifically recognize the guanosine residue of the nucleotide (GTP or GDP) substrate to catalyze the synthesis of the housekeeping alarmone (p)ppGpp (Figure 7A). In toxic SAS enzymes such as *C. marina* FaRel and *P. aeruginosa* Tas1, the substrate specificity is either relaxed, allowing synthesis of both (p)ppGpp and (pp)pApp (toxSAS FaRel; Jimmy et al., 2020), or switched to specific synthesis of (pp)pApp (Tas1; Ahmad et al., 2019) (Figure 7B).

As we show here, the majority of toxSAS pyrophosphorylate tRNA 3′ CCA end to inhibit translation (Figure 7C). In a related

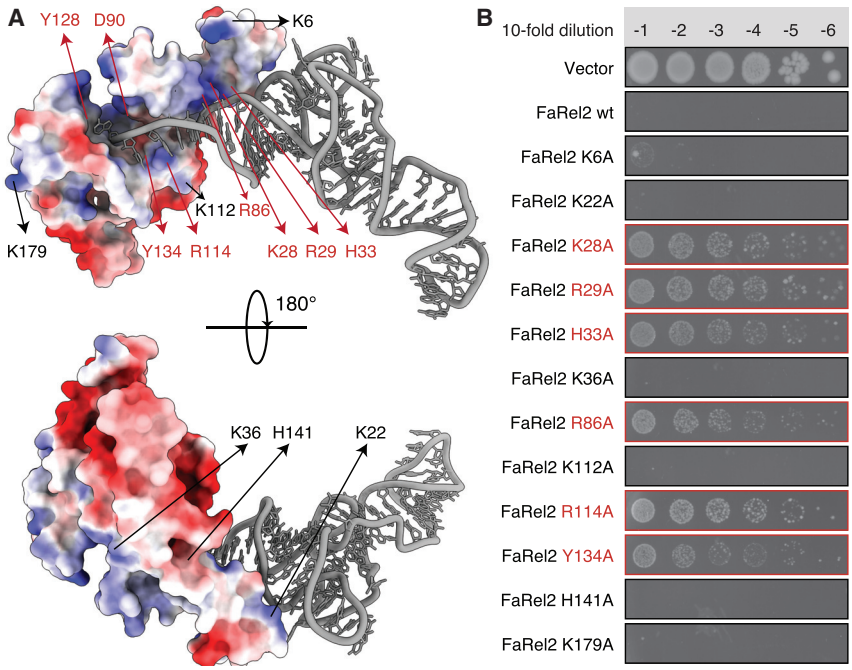

Figure 6. Mutational mapping of the predicted FaRel2: 3′ CCA tRNA interface

(A) Surface representation of the model of the FaRel2:tRNA^{Phe} complex. The surface is colored on the basis of electrostatic potential. The phosphodiester backbone of the bound tRNA^{Phe} complements a cluster of positive charges at the active site exit of the enzyme. The predicted FaRel2:tRNA^{Phe} interface involves residues K28, R29, H33, R86, R114, and Y134. While these guide the CCA end into the active site, functionally essential residue Y128 coordinates the 3′ adenosine of the CCA.

(B) Ten-fold dilutions of overnight cultures of *E. coli* strains transformed with the pBAD33 vector plasmid or derivatives expressing either wild-type *faRel2* or FaRel2 variants with Ala substitutions at the predicted tRNA-binding interface (K28, R29, H33, R86, R114, and Y134), neighboring residues (K6, K22, K112 and H141), and positively charged residues outside the binding region (H36 and K179). The latter were served as negative controls. Substitutions at the predicted tRNA-binding interface specifically abrogate toxicity of FaRel2. Analogous experiments with D90G and Y128A are shown in Figure 1D.

study, we have verified two more additional examples of translation-inhibiting toxSASs from *Vibrio harveyi* and *Lactobacillus animalis* (Kurata et al., 2021). Translation-inhibiting toxSASs belong to SAS subfamilies that are found in various major phyla of Gram-positive and Gram-negative bacteria, including Firmicutes, Actinobacteria, Proteobacteria, Bacteroidetes, Acidobacteria, Planctomycetes, and Cyanobacteria, as well as multiple bacteriophages and even some archaea and fungi (Jimmy et al., 2020). Sequence alignment of the SYNTH domain of toxSASs and other SASs shows that although there are strongly differentially conserved motifs in (pp)pApp-synthesizing toxSASs relative to other RSHs, there is, surprisingly, not a clear sequence signature of toxSASs that use tRNA as a substrate (Figure S5). Indeed, there is no particular support for monophyly of all toxSASs targeting translation in phylogenetic analysis of RSHs, although there is support for two monophyletic clades comprising CapRel+PhRel and FaRel2+PhRel2+FpRel2 (the latter being a sub- or sister group of PhRel2) (Jimmy et al., 2020). The position of the tRNA accepting toxSAS clades at roughly the midpoint of the RSH tree tempts us to speculate that the ancestral function of the SYNTH domain at a time predating the last universal common ancestor (LUCA) could have been pyrophosphorylation of RNA, rather than (pp)pNpp synthesis.

With 30 distinct SAS subfamilies identified to date (Jimmy et al., 2020), it is likely that we are yet to discover the full spectrum of chemical reactions catalyzed by the evolutionary versatile RSH synthetase domain. As we show here, the pyrophosphorylated tRNA 3′ CCA end can serve as a substrate for the SAH enzymes human MESH1 and *C. marina* ATfaRel (Figure 5B). This expands the spectrum of known hydrolysis reactions catalyzed by RSH beyond hydrolysis of pyrophosphorylated nucleotides, indicating a possible role of RSH hydrolases as RNA-modifying enzymes with a 3′-phosphatase activity similar to that of T4 polynucleotide kinase, Pnk.

Limitations of the study

Further studies of non-alarmone chemistry catalyzed by bacterial and viral RSH enzymes are warranted. Dedicated structural studies are essential for further rationalizing our results on the molecular level. All of the experiments presented in the present study rely on heterologous expression in *E. coli* or use a reconstituted biochemical system from *E. coli* components. In order to understand the biological roles of toxSAS TAs, it will be essential to study these effectors and the antitoxins neutralizing them in native bacterial and viral hosts. Finally, exhaustive tRNA specificity studies similar to those undertaken for GNAT AtaT TA toxins (Yashiro et al., 2020) are necessary in order to establish the specific cellular tRNA species targeted by translation-targeting toxSAS toxins.

STAR★METHODS

Detailed methods are provided in the online version of this paper and include the following:

- KEY RESOURCES TABLE
- RESOURCE AVAILABILITY
  - Lead contact
  - Materials availability
  - Data and code availability
- EXPERIMENTAL MODEL AND SUBJECT DETAILS
  - Bacterial strains
- METHOD DETAILS
  - Multiple sequence alignment

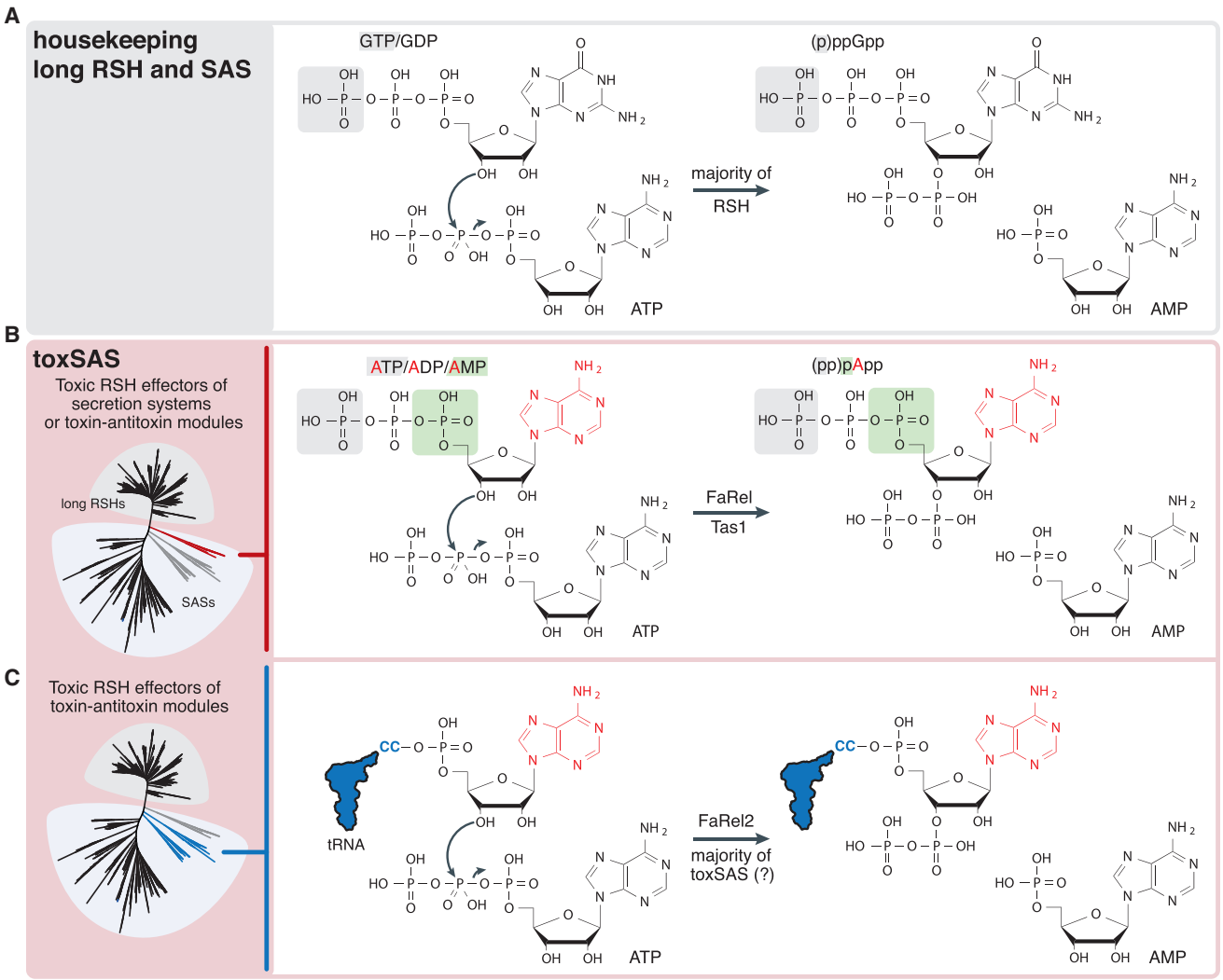

Figure 7. RSH differences in substrate specificity, from nucleotide-mediated signaling via production of (p)ppGpp and (pp)pApp alarmones to toxic modification of the tRNA 3′ CCA end.

(A) Housekeeping RSHs synthesize (p)ppGpp by transferring the pyrophosphate group of ATP onto the 3′ ribose position of either GDP or GTP and degrade the alarmone by hydrolyzing the nucleotide back to GDP or GTP.

(B) The substrate specificity of the Tas1 toxic SAS secretion system effectors and FaRel toxic components of toxin-antitoxin systems deviate from strict recognition of the guanine moiety of GDP/GTP used by "housekeeping" RSHs in favor of the adenine moiety of ATP/ADT/AMP to produce toxic (pp)pApp alarmones.

(C) The majority of identified toxSAS subfamilies specifically inhibit protein synthesis. FaRel2 toxic components of toxin-antitoxin systems recognize the adenine moiety of tRNA 3′ CCA instead of ATP/ADT/AMP nucleotides and transfer the pyrophosphate group of ATP onto the 3′ ribose position tRNA 3′ terminal adenosine. This modification abrogates both tRNA aminoacylation and recognition by the amino acid sensor RSH RelA. Phylogenetic trees are as constructed previously (Jimmy et al., 2020).

- Construction of plasmids
- Synthesis and characterization of (pp)pApp
- ppApp 11a
- pppApp 11b
- pApp 15
- HPLC-based nucleotide quantification
- Metabolic labeling with ^{35}S-methionine, ^{3}H-uridine or ^{3}H-thymidine
- Toxicity validation assays
- Sucrose gradient fractionation
- Protein expression and purification
- Preparation of *E. coli* fMet-tRNA$_i^{fMet}$ and tRNA^{Phe} modified by Coprobacillus sp. D7 FaRel2
- Biochemical assays
- Mass spectrometry
- Structural modeling and docking
- Figure preparation

● QUANTIFICATION AND STATISTICAL ANALYSIS

SUPPLEMENTAL INFORMATION

Supplemental information can be found online at https://doi.org/10.1016/j.molcel.2021.06.005.

ACKNOWLEDGMENTS

We are grateful to Protein Expertise Platform (PEP) at Umeå University and Mikael Lindberg for constructing plasmids; Andrey Chabes, Nasim Sabouri, and Ikenna Obi for providing γ-^{32}P ATP; and Steffi Jimmy and Constantine Stavropoulos their contributions at the initial stages of this project. This work was supported by funds from European Regional Development Fund through the Centre of Excellence for Molecular Cell Technology (V.H. and T.T.; 2014-2020.4.01.15-0013); Molecular Infection Medicine Sweden (MIMS) (V.H.); the Estonian Research Council (PRG335 to T.T. and V.H.); Molecular Infection Biology Estonia – Research Capacity Building Project (H2020-WIDESPREAD-2018-2020/GA: 857518 to T.T. and V.H.); the Swedish Research Council (Vetenskapsrådet; 2017-03783 to V.H. and 2019-01085 to G.C.A.); the Ragnar Söderberg Foundation (V.H.); the MIMS Excellence by Choice Postdoctoral Fellowship Programme (postdoctoral grant 2018 to M.R.); the Kempe Foundation (SMK-1858.3 to G.C.A.); Carl Tryggers Stiftelse för Vetenskaplig Forskning (19-24 to G.C.A.); the Czech Ministry of Education and Sport (grant 8F19006 to D.R.); the Swedish Research Council (2018-00956 to V.H.) within the RIBOTARGET consortium under the framework of the Joint Programming Initiative on Antimicrobial Resistance (JPIAMR); Umeå Centre for Microbial Research (UCMR) (postdoctoral grant 2017 to H. Takada); Grants-in-Aid for Scientific Research from the Japan Society for the Promotion of Science (JSPS) (18H05272 to T.S.); Exploratory Research for Advanced Technology (ERATO) from the Japan Science and Technology Agency (JST) (JPMJER2002 to T.S.); Fonds National de Recherche Scientifique (FRFS-WELBIO CR-2017S-03, FNRS CDR J.0068.19, and FNRS-PDR T.0066.18); JPIAMR (JPI-EC-AMR-R.8004.18); Program Actions de Recherche Concerté 2016–2021 and Fonds d'Encouragement à la Recherche (FER) of Université libre de Bruxelles (ULB); Fonds Jean Brachet, Fondation Van Buuren, and the European Research Council (ERC) Consolidator Grant (CoG) DiStRes (grant agreement 864311) to A.G.-P.; the European Union's Horizon 2020 research and innovation program under Marie Skłodowska-Curie grant agreement 801505 (IF@ULB postdoctoral grant to A.A.).

AUTHOR CONTRIBUTIONS

V.H. coordinated the study and drafted the manuscript with contributions from all authors. T.K., T.S., A.G.-P., and V.H. designed experiments and analyzed the data. T.K., T.B., S.R.A.O., M.R., K.J.T., Y.S., O.B., A.A., H. Takada, and H. Taman performed experiments. D.R., R.P., T.T., and A.G.-P. provided reagents. G.C.A. performed bioinformatic analyses.

DECLARATION OF INTERESTS

The authors declare no competing interests.

Received: December 18, 2020
Revised: April 28, 2021
Accepted: June 2, 2021
Published: June 25, 2021

REFERENCES

Ahmad, S., Wang, B., Walker, M.D., Tran, H.R., Stogios, P.J., Savchenko, A., Grant, R.A., McArthur, A.G., Laub, M.T., and Whitney, J.C. (2019). An interbacterial toxin inhibits target cell growth by synthesizing (p)ppApp. Nature *575*, 674–678.

Akichika, S., Hirano, S., Shichino, Y., Suzuki, T., Nishimasu, H., Ishitani, R., Sugita, A., Hirose, Y., Iwasaki, S., Nureki, O., and Suzuki, T. (2019). Cap-specific terminal N^6-methylation of RNA by an RNA polymerase II-associated methyltransferase. Science *363*, eaav0080.

Arenz, S., Abdelshahid, M., Sohmen, D., Payoe, R., Starosta, A.L., Berninghausen, O., Hauryliuk, V., Beckmann, R., and Wilson, D.N. (2016). The stringent factor RelA adopts an open conformation on the ribosome to stimulate ppGpp synthesis. Nucleic Acids Res. *44*, 6471–6481.

Atkinson, G.C., Tenson, T., and Hauryliuk, V. (2011). The RelA/SpoT homolog (RSH) superfamily: distribution and functional evolution of ppGpp synthetases and hydrolases across the tree of life. PLoS ONE *6*, e23479.

Blower, T.R., Fineran, P.C., Johnson, M.J., Toth, I.K., Humphreys, D.P., and Salmond, G.P. (2009). Mutagenesis and functional characterization of the RNA and protein components of the toxIN abortive infection and toxin-antitoxin locus of Erwinia. J. Bacteriol. *191*, 6029–6039.

Brosius, J., and Holy, A. (1984). Regulation of ribosomal RNA promoters with a synthetic *lac* operator. Proc. Natl. Acad. Sci. U S A *81*, 6929–6933.

Brown, A., Fernández, I.S., Gordiyenko, Y., and Ramakrishnan, V. (2016). Ribosome-dependent activation of stringent control. Nature *534*, 277–280.

Burckhardt, R.M., and Escalante-Semerena, J.C. (2020). Small-molecule acetylation by GCN5-related *N*-acetyltransferases in bacteria. Microbiol. Mol. Biol. Rev. *84*, e00090-19.

Cai, Y., Usher, B., Gutierrez, C., Tolcan, A., Mansour, M., Fineran, P.C., Condon, C., Neyrolles, O., Genevaux, P., and Blower, T.R. (2020). A nucleotidyltransferase toxin inhibits growth of *Mycobacterium tuberculosis* through inactivation of tRNA acceptor stems. Sci. Adv. *6*, eabb6651.

Candiano, G., Bruschi, M., Musante, L., Santucci, L., Ghiggeri, G.M., Carnemolla, B., Orecchia, P., Zardi, L., and Righetti, P.G. (2004). Blue silver: a very sensitive colloidal Coomassie G-250 staining for proteome analysis. Electrophoresis *25*, 1327–1333.

Cashel, M., and Gallant, J. (1969). Two compounds implicated in the function of the RC gene of *Escherichia coli*. Nature *221*, 838–841.

Castro-Roa, D., Garcia-Pino, A., De Gieter, S., van Nuland, N.A.J., Loris, R., and Zenkin, N. (2013). The Fic protein Doc uses an inverted substrate to phosphorylate and inactivate EF-Tu. Nat. Chem. Biol. *9*, 811–817.

Cheverton, A.M., Gollan, B., Przydacz, M., Wong, C.T., Mylona, A., Hare, S.A., and Helaine, S. (2016). A salmonella toxin promotes persister formation through acetylation of tRNA. Mol. Cell *63*, 86–96.

Cruz, J.W., Sharp, J.D., Hoffer, E.D., Maehigashi, T., Vvedenskaya, I.O., Konkimalla, A., Husson, R.N., Nickels, B.E., Dunham, C.M., and Woychik, N.A. (2015). Growth-regulating *Mycobacterium tuberculosis* VapC-mt4 toxin is an isoacceptor-specific tRNase. Nat. Commun. *6*, 7480.

Dedrick, R.M., Jacobs-Sera, D., Bustamante, C.A., Garlena, R.A., Mavrich, T.N., Pope, W.H., Reyes, J.C., Russell, D.A., Adair, T., Alvey, R., et al. (2017). Prophage-mediated defence against viral attack and viral counter-defence. Nat. Microbiol. *2*, 16251.

Ding, C.C., Rose, J., Sun, T., Wu, J., Chen, P.H., Lin, C.C., Yang, W.H., Chen, K.Y., Lee, H., Xu, E., et al. (2020). MESH1 is a cytosolic NADPH phosphatase that regulates ferroptosis. Nat. Metab. *2*, 270–277.

Ennis, H.L. (1972). Polysome metabolism in *Escherichia coli*: effect of antibiotics on polysome stability. Antimicrob. Agents Chemother. *1*, 197–203.

Fiedoruk, K., Daniluk, T., Swiecicka, I., Sciepuk, M., and Leszczynska, K. (2015). Type II toxin-antitoxin systems are unevenly distributed among *Escherichia coli* phylogroups. Microbiology (Reading) *161*, 158–167.

Fraikin, N., Goormaghtigh, F., and Van Melderen, L. (2020). Type II toxin-antitoxin systems: evolution and revolutions. J. Bacteriol. *202*, e00763-19.

Gaca, A.O., Colomer-Winter, C., and Lemos, J.A. (2015). Many means to a common end: the intricacies of (p)ppGpp metabolism and its control of bacterial homeostasis. J. Bacteriol. *197*, 1146–1156.

Garcia-Pino, A., Zenkin, N., and Loris, R. (2014). The many faces of Fic: structural and functional aspects of Fic enzymes. Trends Biochem. Sci. *39*, 121–129.

Geiger, T., Kästle, B., Gratani, F.L., Goerke, C., and Wolz, C. (2014). Two small (p)ppGpp synthases in *Staphylococcus aureus* mediate tolerance against cell envelope stress conditions. J. Bacteriol. *196*, 894–902.

Goddard, T.D., Huang, C.C., Meng, E.C., Pettersen, E.F., Couch, G.S., Morris, J.H., and Ferrin, T.E. (2018). UCSF ChimeraX: meeting modern challenges in visualization and analysis. Protein Sci. *27*, 14–25.

Goeders, N., Drèze, P.L., and Van Melderen, L. (2013). Relaxed cleavage specificity within the RelE toxin family. J. Bacteriol. *195*, 2541–2549.

Grenier, F., Matteau, D., Baby, V., and Rodrigue, S. (2014). Complete genome sequence of *Escherichia coli* BW25113. Genome Announc. *2*, e01038-14.

Guegler, C.K., and Laub, M.T. (2021). Shutoff of host transcription triggers a toxin-antitoxin system to cleave phage RNA and abort infection. Mol. Cell *81*, 2361–2373.e9.

Guzman, L.M., Belin, D., Carson, M.J., and Beckwith, J. (1995). Tight regulation, modulation, and high-level expression by vectors containing the arabinose P_{BAD} promoter. J. Bacteriol. *177*, 4121–4130.

Harms, A., Stanger, F.V., Scheu, P.D., de Jong, I.G., Goepfert, A., Glatter, T., Gerdes, K., Schirmer, T., and Dehio, C. (2015). Adenylylation of gyrase and Topo IV by FicT toxins disrupts bacterial DNA topology. Cell Rep. *12*, 1497–1507.

Harms, A., Brodersen, D.E., Mitarai, N., and Gerdes, K. (2018). Toxins, targets, and triggers: an overview of toxin-antitoxin biology. Mol. Cell *70*, 768–784.

Haseltine, W.A., and Block, R. (1973). Synthesis of guanosine tetra- and pentaphosphate requires the presence of a codon-specific, uncharged transfer ribonucleic acid in the acceptor site of ribosomes. Proc. Natl. Acad. Sci. U S A *70*, 1564–1568.

Hauryliuk, V., Atkinson, G.C., Murakami, K.S., Tenson, T., and Gerdes, K. (2015). Recent functional insights into the role of (p)ppGpp in bacterial physiology. Nat. Rev. Microbiol. *13*, 298–309.

Hogg, T., Mechold, U., Malke, H., Cashel, M., and Hilgenfeld, R. (2004). Conformational antagonism between opposing active sites in a bifunctional RelA/SpoT homolog modulates (p)ppGpp metabolism during the stringent response. Cell *117*, 57–68.

Irving, S.E., Choudhury, N.R., and Corrigan, R.M. (2021). The stringent response and physiological roles of (pp)pGpp in bacteria. Nat. Rev. Microbiol. *19*, 256–271.

Jaffé, A., Ogura, T., and Hiraga, S. (1985). Effects of the ccd function of the F plasmid on bacterial growth. J. Bacteriol. *163*, 841–849.

Jaskólska, M., and Gerdes, K. (2015). CRP-dependent positive autoregulation and proteolytic degradation regulate competence activator Sxy of *Escherichia coli*. Mol. Microbiol. *95*, 833–845.

Jimmy, S., Saha, C.K., Kurata, T., Stavropoulos, C., Oliveira, S.R.A., Koh, A., Cepauskas, A., Takada, H., Rejman, D., Tenson, T., et al. (2020). A widespread toxin-antitoxin system exploiting growth control via alarmone signaling. Proc. Natl. Acad. Sci. U S A *117*, 10500–10510.

Jurenaite, M., Markuckas, A., and Suziedeliene, E. (2013). Identification and characterization of type II toxin-antitoxin systems in the opportunistic pathogen *Acinetobacter baumannii*. J. Bacteriol. *195*, 3165–3172.

Jurėnas, D., Chatterjee, S., Konijnenberg, A., Sobott, F., Droogmans, L., Garcia-Pino, A., and Van Melderen, L. (2017). AtaT blocks translation initiation by N-acetylation of the initiator $tRNA^{fMet}$. Nat. Chem. Biol. *13*, 640–646.

Katoh, K., and Standley, D.M. (2013). MAFFT multiple sequence alignment software version 7: improvements in performance and usability. Mol. Biol. Evol. *30*, 772–780.

Koonin, E.V., and Makarova, K.S. (2019). Origins and evolution of CRISPR-Cas systems. Philos. Trans. R. Soc. Lond. B Biol. Sci. *374*, 20180087.

Kudrin, P., Varik, V., Oliveira, S.R., Beljantseva, J., Del Peso Santos, T., Dzhygyr, I., Rejman, D., Cava, F., Tenson, T., and Hauryliuk, V. (2017). Subinhibitory concentrations of bacteriostatic antibiotics induce *relA*-dependent and *relA*-independent tolerance to β-lactams. Antimicrob. Agents Chemother. *61*, e02173-16.

Kudrin, P., Dzhygyr, I., Ishiguro, K., Beljantseva, J., Maksimova, E., Oliveira, S.R.A., Varik, V., Payoe, R., Konevega, A.L., Tenson, T., et al. (2018). The ribosomal A-site finger is crucial for binding and activation of the stringent factor RelA. Nucleic Acids Res. *46*, 1973–1983.

Kurata, T., Saha, C.K., Buttress, J.A., Mets, T., Brodiazhenko, T., Turnbull, K.J., Awoyomi, A.F., Oliveira, S.R.A., Jimmy, S., Ernits, K., et al. (2021). Panacea: a hyperpromiscuous antitoxin protein domain for the neutralisation of diverse toxin domains. bioRxiv. https://doi.org/10.1101/2021.05.07.442387.

Lima-Mendez, G., Oliveira Alvarenga, D., Ross, K., Hallet, B., Van Melderen, L., Varani, A.M., and Chandler, M. (2020). Toxin-antitoxin gene pairs found in Tn *3* family transposons appear to be an integral part of the transposition module. MBio *11*, e00452-20.

Liu, K., Bittner, A.N., and Wang, J.D. (2015). Diversity in (p)ppGpp metabolism and effectors. Curr. Opin. Microbiol. *24*, 72–79.

Loveland, A.B., Bah, E., Madireddy, R., Zhang, Y., Brilot, A.F., Grigorieff, N., and Korostelev, A.A. (2016). Ribosome●RelA structures reveal the mechanism of stringent response activation. eLife *5*, e17029.

Manav, M.C., Beljantseva, J., Bojer, M.S., Tenson, T., Ingmer, H., Hauryliuk, V., and Brodersen, D.E. (2018). Structural basis for (p)ppGpp synthesis by the *Staphylococcus aureus* small alarmone synthetase RelP. J. Biol. Chem. *293*, 3254–3264.

Murina, V., Kasari, M., Hauryliuk, V., and Atkinson, G.C. (2018). Antibiotic resistance ABCF proteins reset the peptidyl transferase centre of the ribosome to counter translational arrest. Nucleic Acids Res. *46*, 3753–3763.

Nanamiya, H., Kasai, K., Nozawa, A., Yun, C.S., Narisawa, T., Murakami, K., Natori, Y., Kawamura, F., and Tozawa, Y. (2008). Identification and functional analysis of novel (p)ppGpp synthetase genes in *Bacillus subtilis*. Mol. Microbiol. *67*, 291–304.

Neidhardt, F.C., Bloch, P.L., and Smith, D.F. (1974). Culture medium for enterobacteria. J. Bacteriol. *119*, 736–747.

Nissen, P., Kjeldgaard, M., Thirup, S., Polekhina, G., Reshetnikova, L., Clark, B.F., and Nyborg, J. (1995). Crystal structure of the ternary complex of $Phe\text{-}tRNA^{Phe}$, EF-Tu, and a GTP analog. Science *270*, 1464–1472.

Page, R., and Peti, W. (2016). Toxin-antitoxin systems in bacterial growth arrest and persistence. Nat. Chem. Biol. *12*, 208–214.

Patil, P.R., Vithani, N., Singh, V., Kumar, A., and Prakash, B. (2020). A revised mechanism for (p)ppGpp synthesis by Rel proteins: the critical role of the 2′-OH of GTP. J. Biol. Chem. *295*, 12851–12867.

Schattenkerk, C., Wreesmann, C.T., van der Marel, G.A., and van Boom, J.H. (1985). Synthesis of riboguanosine pentaphosphate ppprGpp (Magic Spot II) via a phosphotriester approach. Nucleic Acids Res. *13*, 3635–3649.

Schneider, C.A., Rasband, W.S., and Eliceiri, K.W. (2012). NIH Image to ImageJ: 25 years of image analysis. Nat. Methods *9*, 671–675.

Schureck, M.A., Dunkle, J.A., Maehigashi, T., Miles, S.J., and Dunham, C.M. (2015). Defining the mRNA recognition signature of a bacterial toxin protein. Proc. Natl. Acad. Sci. U S A *112*, 13862–13867.

Senissar, M., Manav, M.C., and Brodersen, D.E. (2017). Structural conservation of the PIN domain active site across all domains of life. Protein Sci. *26*, 1474–1492.

Shimizu, Y., Inoue, A., Tomari, Y., Suzuki, T., Yokogawa, T., Nishikawa, K., and Ueda, T. (2001). Cell-free translation reconstituted with purified components. Nat. Biotechnol. *19*, 751–755.

Song, S., and Wood, T.K. (2020). A primary physiological role of toxin/antitoxin systems is phage inhibition. Front. Microbiol. *11*, 1895.

Song, Y., DiMaio, F., Wang, R.Y., Kim, D., Miles, C., Brunette, T., Thompson, J., and Baker, D. (2013). High-resolution comparative modeling with RosettaCM. Structure *21*, 1735–1742.

Sprinzl, M., and Richter, D. (1976). Free 3′-OH group of the terminal adenosine of the tRNA molecule is essential for the synthesis in vitro of guanosine tetraphosphate and pentaphosphate in a ribosomal system from *Escherichia coli*. Eur. J. Biochem. *71*, 171–176.

Steinchen, W., Schuhmacher, J.S., Altegoer, F., Fage, C.D., Srinivasan, V., Linne, U., Marahiel, M.A., and Bange, G. (2015). Catalytic mechanism and allosteric regulation of an oligomeric (p)ppGpp synthetase by an alarmone. Proc. Natl. Acad. Sci. U S A *112*, 13348–13353.

Steinchen, W., Vogt, M.S., Altegoer, F., Giammarinaro, P.I., Horvatek, P., Wolz, C., and Bange, G. (2018). Structural and mechanistic divergence of the small (p)ppGpp synthetases RelP and RelQ. Sci. Rep. *8*, 2195.

Sun, D., Lee, G., Lee, J.H., Kim, H.Y., Rhee, H.W., Park, S.Y., Kim, K.J., Kim, Y., Kim, B.Y., Hong, J.I., et al. (2010). A metazoan ortholog of SpoT hydrolyzes ppGpp and functions in starvation responses. Nat. Struct. Mol. Biol. *17*, 1188–1194.

Suzuki, T., Ikeuchi, Y., Noma, A., Suzuki, T., and Sakaguchi, Y. (2007). Mass spectrometric identification and characterization of RNA-modifying enzymes. Methods Enzymol. *425*, 211–229.

Suzuki, T., Yashiro, Y., Kikuchi, I., Ishigami, Y., Saito, H., Matsuzawa, I., Okada, S., Mito, M., Iwasaki, S., Ma, D., et al. (2020). Complete chemical structures of human mitochondrial tRNAs. Nat. Commun. *11*, 4269.

Takada, H., Roghanian, M., Murina, V., Dzhygyr, I., Murayama, R., Akanuma, G., Atkinson, G.C., Garcia-Pino, A., and Hauryliuk, V. (2020). The C-terminal RRM/ACT domain is crucial for fine-tuning the activation of 'long' RelA-SpoT homolog enzymes by ribosomal complexes. Front. Microbiol. *11*, 277.

Turnbull, K.J., Dzhygyr, I., Lindemose, S., Hauryliuk, V., and Roghanian, M. (2019). Intramolecular interactions dominate the autoregulation of *Escherichia coli* stringent factor RelA. Front. Microbiol. *10*, 1966.

van Zundert, G.C.P., Rodrigues, J.P.G.L.M., Trellet, M., Schmitz, C., Kastritis, P.L., Karaca, E., Melquiond, A.S.J., van Dijk, M., de Vries, S.J., and Bonvin, A.M.J.J. (2016). The HADDOCK2.2 web server: user-friendly integrative modeling of biomolecular complexes. J. Mol. Biol. *428*, 720–725.

Varik, V., Oliveira, S.R.A., Hauryliuk, V., and Tenson, T. (2017). HPLC-based quantification of bacterial housekeeping nucleotides and alarmone messengers ppGpp and pppGpp. Sci. Rep. *7*, 11022.

Waterhouse, A.M., Procter, J.B., Martin, D.M., Clamp, M., and Barton, G.J. (2009). Jalview Version 2—a multiple sequence alignment editor and analysis workbench. Bioinformatics *25*, 1189–1191.

Weinger, J.S., and Strobel, S.A. (2006). Participation of the tRNA A76 hydroxyl groups throughout translation. Biochemistry *45*, 5939–5948.

Winther, K.S., and Gerdes, K. (2011). Enteric virulence associated protein VapC inhibits translation by cleavage of initiator tRNA. Proc. Natl. Acad. Sci. U S A *108*, 7403–7407.

Xiao, H., Kalman, M., Ikehara, K., Zemel, S., Glaser, G., and Cashel, M. (1991). Residual guanosine 3′,5′-bispyrophosphate synthetic activity of *relA* null mutants can be eliminated by *spoT* null mutations. J. Biol. Chem. *266*, 5980–5990.

Yamaguchi, Y., and Inouye, M. (2009). mRNA interferases, sequence-specific endoribonucleases from the toxin-antitoxin systems. Prog. Mol. Biol. Transl. Sci. *85*, 467–500.

Yashiro, Y., Sakaguchi, Y., Suzuki, T., and Tomita, K. (2020). Mechanism of aminoacyl-tRNA acetylation by an aminoacyl-tRNA acetyltransferase AtaT from enterohemorrhagic *E. coli*. Nat. Commun. *11*, 5438.

Zhu, M., Pan, Y., and Dai, X. (2019). (p)ppGpp: the magic governor of bacterial growth economy. Curr. Genet. *65*, 1121–1125.

STAR★METHODS

KEY RESOURCES TABLE

REAGENT or RESOURCE	SOURCE	IDENTIFIER
Antibodies		
Anti-Flag M2 primary antibodies (1:5,000)	Sigma-Aldrich	Cat#F1804 RRID: AB_262044
Anti-mouse-HRP secondary antibodies (1:10,000)	Rockland	Cat#610-103-040 RRID: AB_2614833
Bacterial strains		
Escherichia coli BW25113	(Grenier et al., 2014)	N/A
E. coli DH5α	Laboratory stock	N/A
For other *E. coli* strains see Table S1	N/A	N/A
Chemicals, peptides, and recombinant proteins		
Anti-FLAG M2 Affinity Gel	Sigma-Aldrich	Cat#A2220-25ML RRID:AB_10063035
Poly FLAG Peptide lyophilized powder	Bimake	Cat#B23112
Phusion High-Fidelity PCR Master Mix with HF Buffer	Thermo Scientific	Cat#F531L
Q5® High-Fidelity DNA Polymerase	New England Biolabs	Cat#M0491L
DpnI	New England Biolabs	Cat#R0176S
T4 DNA Ligase	New England Biolabs	Cat#M0202S
NEBuilder® HiFi DNA Assembly Master Mix	New England Biolabs	Cat#E2621L
L-[^{35}S]-Methionine	PerkinElmer	Cat#NEG009C005MC
[5,6-^{3}H]-Uridine	PerkinElmer	Cat#NET367250UC
[Methyl-^{3}H]-Thymidine	PerkinElmer	Cat#NET027W001MC
ATP, [γ-^{32}P]- 3000Ci/mmol 10mCi/ml EasyTide Lead	PerkinElmer	Cat#NEG502A500UC
L-[2,3,4,5,6-3H]-Phenylalanine	PerkinElmer	Cat#NET1122001MC
EcoLite Liquid Scintillation Cocktail	MP Biomedicals	Cat#01882475-CF
TEV protease	Protein Expertise Platform at Umeå University	N/A
PURExpress *In Vitro* Protein Synthesis Kit	New England Biolabs	Cat#E6800
PURExpress Δ(aa, tRNA) Kit	New England Biolabs	Cat#E6840S
RNase Inhibitor Murine	New England Biolabs	Cat#M0314S
pppGpp	(Takada et al., 2020)	N/A
pApp	This work	N/A
ppApp	(Jimmy et al., 2020)	N/A
pppApp	This work	N/A
^{3}H-ppGpp	(Takada et al., 2020)	N/A
70S initiation complex (IC) (MVF)	(Takada et al., 2020)	N/A
WesternBright Quantum	Advansta	Cat#K-12042-D10
cOmplete EDTA-free Protease Inhibitor Cocktail	Roche	Cat#4693132001
E. coli tRNA^{Phe}	Chemical Block	N/A
E. coli tRNA^{Val}	Chemical Block	N/A
E. coli tRNA$_i^{Met}$	Chemical Block	N/A
Oligonucleotides		
For primers used for cloning of *E. coli* plasmids see Table S1	N/A	N/A
5′ rCrArCrCrA 3′	Integrated DNA Technologies	N/A

(*Continued on next page*)

Continued

REAGENT or RESOURCE	SOURCE	IDENTIFIER
5′ rCrArCrCrU 3′	Integrated DNA Technologies	N/A
5′ rCrArCrCrG 3′	Integrated DNA Technologies	N/A
5′ rCrArCrCrC 3′	Integrated DNA Technologies	N/A
5′ dCdAdCdCdA 3′	Integrated DNA Technologies	N/A
Recombinant DNA		
For *E. coli* vectors see Table S1	This work	N/A
Software and algorithms		
Rosetta	(Song et al., 2013)	RRID:SCR_015701
HADDOCK	(van Zundert et al., 2016)	RRID:SCR_019091
MAFFT	(Katoh and Standley, 2013)	RRID:SCR_011811
Jalview	(Waterhouse et al., 2009)	RRID:SCR_006459
UCSF ChimeraX	(Goddard et al., 2018)	RRID:SCR_015872
Other		
FastPrep-24 classic	MP Biomedicals	https://www.mpbio.com
Biocomp Gradient Station	BioComp Instruments	http://www.biocompinstruments.com
Trans-Blot Turbo 0.2 μm Midi Nitrocellulose Transfer Pack	Bio-Rad	Cat#1704159
ImageQuant LAS 4000	GE Healthcare	https://www.cytivalifesciences.com
Mix2Seq sequencing service	Eurofins Genomics	https://eurofinsgenomics.eu
Micro Bio-Spin Columns	Bio-Rad	Cat#7326204
Typhoon FLA 9500	GE Healthcare	https://www.cytivalifesciences.com
0.1 mm Zirconium beads	BioSpec	Cat#11079101z
Multi-Purpose Tube Rotators	Fisherbrand	https://www.fishersci.com
Micro Bio-Spin Columns	Bio-Rad	Cat#7326204
HisTrap 1 mL HP column	GE Healthcare	Cat#17-5247-01
HisTrap 5 mL HP column	GE Healthcare	Cat#17-5248-01
HiPrep 10/26 desalting column	GE Healthcare	Cat#17-5087-01
HiLoad 16/600 Superdex 200 pg column	GE Healthcare	Cat#28-9893-35
POLYGRAM CEL 300 PEI	Machery Nagel	Cat#801053, Lot#01.17
ÄKTA avant 25	GE Healthcare	https://www.cytivalifesciences.com

RESOURCE AVAILABILITY

Lead contact

Please direct any requests for further information or reagents to the Lead Contact: Vasili Hauryliuk (vasili.hauryliuk@med.lu.se).

Materials availability

All unique/stable reagents generated in this study are available from the Lead Contact without restriction.

Data and code availability

The study does not make use of unpublished data or software. Phylogenetic trees are revisualized versions of those previously generated (Jimmy et al., 2020).

Sequences shown in the multiple sequence alignment of Figure S5A can be downloaded from the Uniprot database (https://www.uniprot.org/) in case of Rel and RelA, and the NCBI protein database for all other sequences, using the accession numbers shown in the figure.

EXPERIMENTAL MODEL AND SUBJECT DETAILS

Bacterial strains

Bacterial strains and plasmids as well as oligonucleotide primers used in the study are listed in Table S1.

CellPress
OPEN ACCESS

METHOD DETAILS

Multiple sequence alignment

Sequences were extracted from the RSH database (Jimmy et al., 2020), aligned with MAFFT v7.164b with the L-ins-i strategy (Katoh and Standley, 2013), and alignments were visualized with Jalview (Waterhouse et al., 2009).

Construction of plasmids

Oligonucleotides were synthesized by Metabion and Sigma. To construct the plasmids, DNA fragments were amplified by PCR and assembled by NEBuilder HiFi DNA Assembly Cloning Kit (NEB, E5520S).

To construct VHp770, DNA fragments were amplified by PCR using VHp277 as a template as well as sets of primers VTK69 and VTK133 or VTK19 and VTK132. To construct VHp701, VHp308 (Jimmy et al., 2020) and pET24d were used as PCR templates with primer sets of VTK80 and VTK83 or VTK63 and VTK81 respectively. To generate VHp771, the DNA fragments were amplified by PCR using VHp678 as the template and sets of primers VTK69 and VTK133 or VTK19 and VTK132. To construct VHp679, VHp366 and VHp678 were used as PCR templates with primers VTK51 and VTK45 or VTK19 and VTK43, respectively. The identity of the constructed plasmids was confirmed through re-sequencing (LGC genomics).

VHp818 and VHp816 were constructed by sub-cloning *faRel* and *faRel2* from VHp307 (Jimmy et al., 2020) and VHp227 (Jimmy et al., 2020), respectively, into pMR33 using the restriction enzymes SacI and HindIII. The constructed plasmids were validated through sequencing (LGC genomics). The point mutations to *faRel2* was done in the plasmid VHp277 background and introduced by amplifying the entire plasmid with divergent primers listed in Table S1. The forward primer introduced the desired amino-acid substitution in its unbound 5′ region. After PCR with Q5 polymerase (NEB), the product was treated with DpnI (NEB) to remove the template plasmid, purified trough a PCR purification column (Omega), phosphorylated with PNK (NEB) and ligated (NEB). The mixture was transformed into *E. coli* MC1061 and the resulting plasmids were verified by sequencing (Eurofins).

Synthesis and characterization of (pp)pApp

The synthesis of (p)ppApp (Figure S2A) followed the same procedure as for the preparation of pppGpp (Schattenkerk et al., 1985) but instead of protected guanosine, N^6-benzoyl adenosine (**1**) was used as the starting material. The final products ((p)ppApp, **11a** and **11b**) were purified by preparative reversed phase HPLC using linear gradient of methanol in 0.1M aqueous TEAB. Triethylammonium salt was converted to potassium salt by passing through small column with Dowex 50 in K^+ phase, lyophilised from water and characterized by NMR and HR-MS. The synthesis of ppApp (**11a**) has been described in detail earlier (Jimmy et al., 2020).

The synthesis of pApp followed a slightly different path (Figure S2B). Dibenzyl phosphate was installed to the 5′-position of the protected adenosine **2** by reaction with dibenzyl diisopropylphosphoramidite under tetrazol catalysis, followed by oxidation with 4-chloroperbenzoic acid. Removal of the levulinyl protecting group was followed by installation of 3′-pyrophosphate using the same methodology as for the synthesis of ppApp.

ppApp 11a

^{1}H NMR (500.2 MHz, D_2O, ref(*t*BuOH) = 1.24 ppm): 4.21 – 4.27 (m, 2H, H-5); 4.59 (p, 1H, $J_{4',3'} = J_{4',5'} = J_{H,P}$ = 2.9, H-4′); 4.88 (ddd, 1H, $J_{2',1'}$ = 6.5, $J_{2',3'}$ = 5.0, $J_{H,P}$ = 1.3, H-2′); 4.98 (ddd, 1H, $J_{H,P}$ = 8.3, $J_{3',2'}$ = 5.0, $J_{3',4'}$ = 2.9, H-3′); 6.22 (d, 1H, $J_{1',2'}$ = 6.5, H-1′); 8.28 (s, 1H, H-2); 8.57 (s, 1H, H-8).

^{13}C NMR (125.8 MHz, D_2O, ref(*t*BuOH) = 32.43 ppm): 67.93 (d, $J_{C,P}$ = 5.3, CH_2-5′); 76.54 (d, $J_{C,P}$ = 4.5, CH-2′); 77.75 (d, $J_{C,P}$ = 5.2, CH-3′); 86.41 (dd, $J_{C,P}$ = 9.1, 3.8, CH-4′); 89.37 (CH-1′); 121.50 (C-5); 142.82 (CH-8); 152.17 (C-4); 155.73 (CH-2); 158.50 (C-6).

^{31}P{^{1}H} NMR (202.5 MHz, D_2O): −10.43 (d, J = 21.8, P_α-3′); −10.33 (d, J = 20.7, P_α-5′); −8.20 (bd, J = 20.7, P_β-5′); −6.45 (bd, J = 21.8, P_β-3′).

IR ν_{max} (KBr) 3436 (versus, br), 3250 (m, br, sh), 3155 (m, br, sh), 1636 (m, br), 1578 (w, sh), 1475 (w, br, sh), 1337 (vw), 1301 (vw), 1220 (w, br), 1103 (w, br), 1074 (w, br), 972 (w, br), 921 (w, br), 797 (vw).

HR-MS(ESI$^-$) For $C_{10}H_{16}O_{16}N_5P_4$ $(M\text{-}H)^-$ calcd 585.95480, found 585.95518.

pppApp 11b

^{1}H NMR (500.2 MHz, D_2O, ref(*t*BuOH) = 1.24 ppm): 4.25 (ddd, 1H, J_{gem} = 11.7, $J_{H,P}$ = 4.9, $J_{5'b,4'}$ = 2.8, H-5′a); 4.28 (ddd, 1H, J_{gem} = 11.7, $J_{H,P}$ = 5.7, $J_{5'a,4'}$ = 2.8, H-5′a); 4.65 (p, 1H, $J_{4',3'} = J_{4',5'} = J_{H,P}$ = 2.8, H-4′); 4.87 (ddd, 1H, $J_{2',1'}$ = 7.0, $J_{2',3'}$ = 5.2, $J_{H,P}$ = 1.3, H-2′); 4.96 (bm, 1H, H-3′); 6.19 (d, 1H, $J_{1',2'}$ = 7.0, H-1′); 8.27 (s, 1H, H-2); 8.56 (s, 1H, H-8).

^{13}C NMR (125.8 MHz, D_2O, ref(*t*BuOH) = 32.43 ppm): 68.38 (d, $J_{C,P}$ = 5.2, CH_2-5′); 76.66 (d, $J_{C,P}$ = 4.9, CH-2′); 78.21 (d, $J_{C,P}$ = 6.0, CH-3′); 86.45 (dd, $J_{C,P}$ = 8.7, 2.9, CH-4′); 89.08 (CH-1′); 121.48 (C-5); 142.81 (CH-8); 152.25 (C-4); 155.66 (CH-2); 158.45 (C-6).

^{31}P{^{1}H} NMR (202.5 MHz, D_2O): −22.14 (t, J = 19.1, P_β-5′); −10.83 (d, J = 20.6, P_α-3′); −10.63 (d, J = 19.1, P_α-5′); −9.65 (bd, J = 19.1, P_γ-5′); −8.63 (bd, J = 20.6, P_β-3′).

HR-MS(ESI$^-$) For $C_{10}H_{17}O_{19}N_5P_5$ $(M\text{-}H)^-$ calcd 665.92113, found 665.91960.

pApp 15

^{1}H NMR (500.2 MHz, D_2O, ref(*t*BuOH) = 1.24 ppm): 4.12 (ddd, 1H, J_{gem} = 11.8, $J_{H,P}$ = 4.6, $J_{5'b,4'}$ = 2.8, H-5′a); 4.16 (ddd, 1H, J_{gem} = 11.8, $J_{H,P}$ = 4.8, $J_{5'a,4'}$ = 2.8, H-5′a); 4.59 (dt, 1H, $J_{4',3'}$ = 3.2, $J_{4',5'}$ = 2.8, H-4′); 4.85 (ddd, 1H, $J_{2',1'}$ = 6.2, $J_{2',3'}$ = 5.1, $J_{H,P}$ = 1.3, H-2′); 4.96 (ddd, 1H, $J_{H,P}$ = 8.5, $J_{3',2'}$ = 5.1, $J_{3',4'}$ = 3.2, H-3′); 6.19 (d, 1H, $J_{1',2'}$ = 6.2, H-1′); 8.26 (s, 1H, H-2); 8.53 (s, 1H, H-8).

^{13}C NMR (125.8 MHz, D_2O, ref(*t*BuOH) = 32.43 ppm): 67.01 (d, $J_{C,P}$ = 4.7, CH_2-5′); 76.58 (d, $J_{C,P}$ = 4.6, CH-2′); 77.57 (d, $J_{C,P}$ = 5.4, CH-3′); 86.34 (dd, $J_{C,P}$ = 8.9, 4.0, CH-4′); 89.55 (CH-1′); 121.53 (C-5); 142.82 (CH-8); 152.09 (C-4); 155.71 (CH-2); 158.49 (C-6).

^{31}P{^{1}H} NMR (202.5 MHz, D_2O): −10.69 (d, J = 21.1, P_α-3′); −7.94 (d, J = 21.2, P_β-3′); 1.51 (s, P-5′).

HR-MS(ESI$^-$) For $C_{10}H_{15}O_{13}N_5P_3$ $(M-H)^-$ calcd 505.98847, found 505.98861.

HPLC-based nucleotide quantification

E. coli strain BW25113 (Grenier et al., 2014) was transformed with RSH-expressing plasmids (pMR33-faRel, pMR33-faRel2 or pBAD33-phRel2) as well as empty pKK223-3 vector. The starter cultures were pre-grown overnight at 37°C with vigorous shaking (200 rpm) in Neidhardt MOPS minimal media (Neidhardt et al., 1974) supplemented with 0.1% casamino acids, 1 μg/mL thiamine, 1% glucose, 100 μg/mL carbenicillin as well as either 20 μg/mL chloramphenicol (pBAD33–phRel2) or 25 μg/mL kanamycin (pMR33-faRel and pMR33-faRel2). The overnight cultures were diluted to OD_{600} 0.05 in 115 mL of pre-warmed medium MOPS supplemented with 0.5% glycerol as carbon source and grown until OD_{600} ≈0.5 (pMR33-faRel and pMR33-faRel2) or OD_{600} ≈0.2 (pBAD33-phRel2) at 37°C, 200 rpm. At this point 0.2% arabinose was added to induce the expression of the toxin. 26 mL samples were collected for HPLC analyses at 0, 2, 5 and 10 minutes after the addition of arabinose and 1 mM IPTG. Nucleotide extraction and HPLC analyses were performed as described previously (Varik et al., 2017). The OD_{600} measurements were performed in parallel with collection of the samples for HPLC analyses.

Metabolic labeling with ^{35}S-methionine, ^{3}H-uridine or ^{3}H-thymidine

Overnight cultures in defined Neidhardt MOPS minimal media (Neidhardt et al., 1974) supplemented with 1% glucose, 0.1% casamino acids and as well as appropriate antibiotics were inoculated with single colonies of *E. coli* BW25113 cells freshly transformed with pBAD33-based plasmid for L-arabinose-inducible RSH expression as well as the empty pKK223-3 vector. After overnight incubation at 37°C with shaking at 180 rpm, the cultures were diluted to an OD_{600} of 0.05 in 15 mL MOPS minimal media supplemented with 19 amino acids (25 μg/mL, final concentration) but lacking methionine, 0.5% glycerol, as well as appropriate antibiotics. The cultures were grown at 37°C until an OD_{600} of 0.2-0.3 in a water bath with shaking (200 rpm), and expression of toxins was induced with 0.2% L-arabinose. For a zero-point 1 mL of culture was taken and mixed with either 4.35 μCi ^{35}S-methionine (Perkin Elmer), 0.65 μCi ^{3}H-uridine (Perkin Elmer) or 2 μCi ^{3}H-thymidine (Perkin Elmer) immediately before induction. Simultaneously, another 1 mL of culture was taken for OD_{600} measurements. Samples were collected at 2, 5, 10 and 15 minutes post-induction and processed as described above. The incorporation of radioisotopes was quenched 8 minutes after addition of the isotope, by the addition of 200 μL ice-cold 50% trichloroacetic acid (TCA). Samples were filtered through GF/C filters (Whatman) prewashed with 5% TCA, followed by washing twice with 5 mL of ice-cold TCA and, finally, twice with 5 mL of 95% EtOH. The filters were dried at least for two hours at room temperature and the radioactivity was quantified by scintillation using EcoLite Liquid Scintillation Cocktail scintillation cocktail (5 mL per vial, MP Biomedicals, 15 minutes shaking with filters prior to counting) using a TRI-CARB 4910TR 100 V scintillation counter (PerkinElmer).

Toxicity validation assays

The experiments were performed as described earlier (Jimmy et al., 2020). The assays were performed on LB medium (Lennox) plates (VWR). We used *E. coli* BW25113 strain co-transformed with two different plasmid systems for controllable expression of toxins and antitoxin.

First, we used a combination of pKK223-3 (medium copy number, ColE1 origin of replication, Amp^R, antitoxins expressed under the control of P_{Tac} promoter; Brosius and Holy, 1984) and pBAD33 harboring toxin genes (medium copy number, p15A origin of replication, Cml^R, toxins expressed under the control of P_{BAD} promoter; Guzman et al., 1995) (Figures 1D and 6B). The cells were grown in liquid LB medium (BD) supplemented with 100 μg/mL carbenicillin (AppliChem) and 20 μg/mL chloramphenicol (AppliChem), 30 mM K_2HPO_4/KH_2PO_4 (pH 7.4) as well as 1% glucose (repression conditions). Serial ten-fold dilutions were spotted (5 μl per spot) on solid LB plates containing carbenicillin and chloramphenicol in addition to either 1% glucose (repressive conditions), or 0.2% arabinose combined with 1 mM IPTG (induction conditions). Plates were scored after an overnight incubation at 37°C. Sequences were codon-optimized for expression in *E. coli.*

Second, we used pMG25 (high copy number, ColE1 origin of replication (pUC), Amp^R, antitoxin expressed under the control of IPTG inducible $P_{A1/04/03}$ promoter; Jaskólska and Gerdes, 2015) and pBAD-based pMR33 (this work) harboring toxin genes (medium copy number, p15A origin of replication, Kan^R, toxins expressed under the control of P_{BAD} promoter) (Figure 5A). The cells were grown in liquid LB medium (BD) supplemented with 0.2% glucose (repression conditions), 100 μg/mL carbenicillin (AppliChem) and 50 μg/mL kanamycin (AppliChem). Serial dilutions and spotting were performed as described above using solid LB plates supplemented with 0.2% arabinose as well as 100 μg/mL carbenicillin (AppliChem) and 50 μg/mL kanamycin (AppliChem).

Sucrose gradient fractionation

Overnight cultures in defined Neidhardt MOPS minimal media supplemented with 1% glucose, 0.1% casamino acids and as well as appropriate antibiotics were inoculated with single colonies of *E. coli* BW25113 cells freshly transformed with either i) pBAD33-based plasmid for L-arabinose-inducible FaRel2 expression as well as the empty pKK223-3 vector, or ii) just pBAD33 and pKK223-3. After overnight incubation at 37°C with shaking at 180 rpm, the cultures were diluted to an OD_{600} of 0.05 in 60 mL MOPS minimal media supplemented with 0.5% glycerol, 0.1% casamino acids and as well as appropriate antibiotics. At OD_{600} of 0.2-0.3 expression of FaRel2 was induced by addition of 0.2% L-arabinose for 5 or 30 min. After induction the cells from 50 mL culture were collected by centrifugation (4,000 rpm, 10 min, at 4°C in A-4-81 Eppendorf rotor), dissolved in 0.5 mL of HEPES:Polymix buffer (5 mM Mg^{2+} final concentration) supplemented with 1 mM PMSF, lysed using FastPrep homogenizer (MP Biomedicals) (four 20 s pulses at 4.0 m/s with chilling on ice for 1 min between the cycles), and clarified by ultracentrifugation (14,800 rpm for 20 min in Microfuge 22R centrifuge equipped with F241.5P rotor (Beckman Coulter)). Clarified cell lysates were loaded onto 5%–35% sucrose gradients in HEPES:Polymix buffer pH 7.5 (5 mM Mg^{2+} final concentration), subjected to centrifugation (36,000 rpm for 3 hours at 4°C, SW-41Ti Beckman Coulter rotor) and analyzed using Biocomp Gradient Station (BioComp Instruments) with A_{260} as a readout.

Protein expression and purification

The *Coprobacillus* sp. D7 C-terminally $FLAG_3$-tagged FaRel2 (FaRel2-$FLAG_3$) was overexpressed in freshly transformed *E. coli* BL21 DE3 co-transformed with the VHp701 plasmid encoding the non-tagged SAH aTfaRel antitoxin under the pET promoter. Fresh transformants were inoculated to a final OD_{600} of 0.04 in the LB medium (800 mL) supplemented with 100 μg/mL kanamycin and 20 μg/mL chloramphenicol. The cultures were grown at 37°C until an OD_{600} of 0.3, the antitoxin was pre- induced with 0.1 mM IPTG (final concentration) for one hour and the toxin was induced with 0.2% arabinose (final concentration) for an additional one hour at 37°C. The cells were collected by centrifugation (8,000 rpm, 10 minutes at 4°C, JLA-10.500 Beckman Coulter rotor), dissolved in 4 mL of cell suspension buffer (20 mM HEPES:KOH pH 7.5, 95 mM KCl, 5 mM NH_4Cl, 0.5 mM $CaCl_2$, 8 mM putrescine, 1 mM spermidine, 5 mM $Mg(OAc)_2$, 1 mM DTT and cOmplete protease inhibitor (Mini, EDTA-free from Roche)). The cell suspension was divided to 1 mL aliquots, and 200 μL of pre-chilled zirconium beads (0.1 mm) were added in the aliquots. Cellular lysates were prepared by a FastPrep homogenizer (MP Biomedicals) (four 20 s pulses at speed 4.5 mp per second with chilling on ice for 2 minutes between the cycles) and clarified by centrifugation at 21,000 g for 20 minutes at 4°C. The supernatant was carefully collected, avoiding the lipid layer and cellular pellet.

30 mg of total protein (as determined by Bradford assay) of each sample was mixed with 100 μL of ANTI-FLAG M2 Affinity Gel (Sigma-Aldrich) and mixed by rotation for 2 hours at 4°C. The mixture was loaded on a Micro Bio-Spin Chromatography Column (Bio-Rad) and flow-through was collected. The gel in the column was washed five times with 1 mL of cell suspension buffer supplemented with 10% glycerol, and the fraction at final wash was collected. The gel was mixed with 300 μL of cell suspension buffer supplemented with 10% glycerol as well as 0.1 mg/mL Poly FLAG Peptide lyophilised powder (Biotool) in the column by rotation for 40 min at 4°C. The elution fraction was passed through the column by spinning down, and was collected in Eppendorf tube. After this elution step, the gel was suspended with 1x sample buffer (50 mM Tris:HCl pH 6.8, 2% SDS, 0.01% bromophenol blue, 10% glycerol, 10 mM DTT and 2% beta-mercaptoethanol) and collected. 0.5 μL of cell lysate, 0.5 μL of flowthrough, 8 μL of wash, 8 μL of elution fractions and 10 μL of gel suspension were resolved on 15% SDS-PAGE gel.

The SDS-PAGE gel was fixed with fixing solution (50% ethanol and 2% phosphoric acid) for 5 min at room temperature, washed with water for 20 minutes at room temperature twice, and stained with "blue silver" solution (Candiano et al., 2004) (0.12% Brilliant Blue G250 (Sigma-Aldrich, 27815), 10% ammonium sulfate, 10% phosphoric acid, and 20% methanol) overnight at room temperature. After washing with water for 3 hours at room temperature, the gel was analyzed on an ImageQuant LAS 4000 (GE Healthcare) imaging system (Figures S4A and S4D). The concentration of FaRel2-$FLAG_3$ was quantified on SDS-PAGE gels by ImageJ (Schneider et al., 2012) using pure ATfaRel2 as a standard.

For western blotting, the proteins resolved by similar electrophoresis were transferred to 0.2 μm nitrocellulose membrane (Bio-Trace™ NT, Pall) using Trans-Blot® Turbo™ Transfer System (Bio-Rad). To detect $FLAG_3$-tagged protein, the membrane was blocked in PBS-T (1xPBS supplemented with 0.05% Tween-20) with 5% w/v nonfat dry milk at room temperature for one hour, and first antibody incubation was performed for overnight at 4°C in PBS-T anti-Flag M2 (Sigma-Aldrich F1804, batch number #SLCD3524; 1:5000 dilution). After three 5-minute washes in fresh PBS-T, second antibody incubations were performed for one hour at room temperature in PBS-T with Goat anti-Mouse IgG-HRP (Agrisera AS11 1772, batch number #810-103-040; 1:4,000 dilution). Tagged-proteins were detected on an ImageQuant LAS 4000 (GE Healthcare) imaging system using WesternBright Quantum HRP substrate (Advansta).

Coprobacillus sp. D7 N-terminally His_6-TEV-tagged ATfaRel2 was overexpressed in freshly transformed *E. coli* BL21(DE3) with VHp364. Fresh transformants were inoculated to a final OD_{600} of 0.05 in the LB medium (800 mL) supplemented with 100 μg/mL kanamycin. The cultures were grown at 37°C until an OD_{600} of 0.5, induced with 0.4 mM IPTG (final concentration) and grown for an additional one hour at 30°C. The cells were harvested by centrifugation and resuspended in buffer A (300 mM NaCl, 10 mM imidazole, 10% glycerol, 4 mM β-mercaptoethanol, 25 mM HEPES:KOH pH 8.0) supplemented with 0.1 mM PMSF and 1 U/mL of DNase I, and lysed by one passage through a high-pressure cell disrupter (Stansted Fluid Power, 150 MPa). Cell debris was removed by centrifugation (25,000 rpm for 1 hour) and clarified lysate was taken for protein purification. Clarified cell lysate was filtered through a 0.22 μm syringe filter and loaded onto a HisTrap 5 mL HP column pre-equilibrated in buffer A. The column was washed with 5

column volumes (CV) of buffer A and following buffer B (1 M NaCl, 10 mM imidazole, 10% glycerol, 4 mM β-mercaptoethanol, 25 mM HEPES:KOH pH 8.0), and the protein was eluted using a linear gradient (3 CV with 0%–100%) of buffer C (300 mM NaCl, 300 mM imidazole, 10% glycerol, 4mM β-mercaptoethanol, 25 mM HEPES:KOH pH 8.0). Fractions enriched in ATfaRel2 (≈60% buffer C) were pooled totaling approximately 8 mL (Figure S4E). The sample was applied on a HiPrep 10/26 desalting column (GE Healthcare) pre-equilibrated with storage buffer (buffer D; 300 mM KCl, 10% glycerol, 4 mM β-mercaptoethanol, 25 mM HEPES:KOH pH 8.0). The fractions containing ATfaRel2 were collected (about 8 mL in total, (Figure S4F) and concentrated on an Amicon Ultra (Millipore) centrifugal filter device with a 3 kDa cut-off. The purity of protein preparations was assessed by SDS-PAGE (Figure S4G). Protein preparations were aliquoted, frozen in liquid nitrogen and stored at –80°C. Individual single-use aliquots were discarded after the experiment.

The C-terminally $FLAG_3$-tagged *B. subtilis* la1a PhRel2 (PhRel2-$FLAG_3$) was overexpressed in freshly transformed *E. coli* BW25113 co-transformed with the VHp847 plasmid encoding the PaSpo SAH antitoxin under the IPTG-inducible promoter ($P_{A1/04/03}$ promoter). Fresh transformants were inoculated to a final OD_{600} of 0.05 in the LB medium (800 mL) supplemented with 100 μg/mL carbenicillin, 20 μg/mL chloramphenicol and 50 μM IPTG. The cultures were grown at 37°C until an OD_{600} of 0.5, the toxin was induced with 0.2% arabinose (final concentration) for an additional 3 hours at 37°C. The cells were collected by centrifugation (8,000 rpm, 10 minutes at 4°C, JLA-10.500 Beckman Coulter rotor), dissolved in 4 mL of cell suspension buffer (20 mM HEPES:KOH pH 7.5, 95 mM KCl, 5 mM NH_4Cl, 0.5 mM $CaCl_2$, 8 mM putrescine, 1 mM spermidine, 5 mM $Mg(OAc)_2$, 1 mM DTT, and cOmplete, Mini, EDTA-free (Roche)). The cell suspension was divided to 1 mL aliquots, and 200 μL of pre-chilled zirconium beads (0.1 mm) were added in the aliquots. Cellular lysates were prepared by a FastPrep homogenizer (MP Biomedicals) (four 20 s pulses at speed 4.5 mp per second with chilling on ice for 2 minutes between the cycles) and clarified by centrifugation at 21,000 g for 20 minutes at 4°C. The supernatant was carefully collected, avoiding the lipid layer and cellular pellet.

30 mg of total protein (as determined by Bradford assay) of each sample was mixed with 100 μL of ANTI-FLAG M2 Affinity Gel (Sigma-Aldrich) and mixed by rotation for 2 hours at 4°C. The mixture was loaded on a Micro Bio-Spin Chromatography Column (Bio-Rad) and flow-through was collected. The gel in the column was washed with 1 mL of cell suspension buffer including 1 M KCl five times and 1 mL of cell suspension buffer supplemented with 10% glycerol five times, and the fraction at final wash was collected. The gel was mixed with 300 μL of cell suspension buffer supplemented with 10% glycerol and 0.1 mg/mL Poly FLAG Peptide lyophilised powder (Biotool) in the column by rotation for 40 min at 4°C. The elution fraction was passed through the column by spinning down, and was collected in Eppendorf tube. After this elution step, the gel was suspended with 1x sample buffer (50 mM Tris:HCl pH 6.8, 2% SDS, 0.01% bromophenol blue, 10% glycerol, 10 mM DTT and 2% beta-mercaptoethanol) and collected. 0.5 μL of cell lysate, 0.5 μL of flowthrough, 8 μL of wash, 8 μL of elution fractions and 10 μL of gel suspension were resolved on 10% SDS-PAGE gel (Figure S4H).

For purification of RelA *E. coli* BL21 DE3 harboring pET24d:his10-SUMO-relA expression constructs were grown, induced, harvested and lysed as described earlier (Kudrin et al., 2018). Protein purification was performed as previously described (Turnbull et al., 2019).

Expression and purification of *B. subtilis* Rel was performed as described earlier (Takada et al., 2020).

C-terminally His_6-tagged *E. coli* phenylalanyl-tRNA synthetase (PheRS) was overexpressed in *E. coli* BL21 (DE3). Fresh transformants were used to inoculate 3 L cultures of LB medium supplemented with 100 μg/mL ampicillin. The cultures were grown at 37°C until an OD_{600} of 0.5, protein expression was induced with 1 mM IPTG (final concentration) and then the cultures were grown overnight at 37°C. The cells were harvested by centrifugation, resuspended in buffer E (150 mM NaCl, 5 mM $MgCl_2$, 20 mM imidazole, 1 mM β-mercaptoethanol, 20 mM Tris:HCl pH 7.5) supplemented with 1 mM PMSF, and lysed by one passage through a high-pressure cell disrupter. Cell debris was removed by centrifugation and clarified lysate was taken for protein purification. Clarified cell lysate was filtered through a 0.22 μm syringe filter and loaded onto a HisTrap 5 mL HP column pre-equilibrated in buffer E. The column was washed with 20 column volumes (CV) of buffer F (1 M NaCl, 5 mM $MgCl_2$, 20 mM imidazole, 1 mM β-mercaptoethanol, 20 mM Tris:HCl pH 7.5) and following buffer E (5 CV), and the protein was eluted using a linear gradient (30 CV with 0%–100%) of buffer G (150 mM NaCl, 5 mM $MgCl_2$, 500 mM imidazole, 1 mM β-mercaptoethanol, 20 mM Tris:HCl pH 7.5). Fractions enriched in PheRS (≈45% buffer G) were pooled. The sample was applied on a HiPrep 10/26 desalting column (GE Healthcare) pre-equilibrated with storage buffer (buffer H; 100 mM KCl, 2 mM $MgCl_2$, 10% glycerol, 6 mM β-mercaptoethanol, 20 mM Tris:HCl pH 7.5). The fractions containing PheRS were collected. The protein was aliquoted, aliquots plunge-frozen in liquid nitrogen and stored at –80°C. Individual single-use aliquots were discarded after the experiment.

Human MESH1 (VHp487, pET21b-His6-TEV-MESH1) was overexpressed in freshly transformed *E. coli* BL21 DE3 Rosetta (Novagen). Transformants were inoculated to a final OD_{600} of 0.05 in LB medium (400 mL × 2) supplemented with 100 μg/mL Carbenicillin. The cultures were grown at 37°C until an OD_{600} of 0.5, induced with 1 mM IPTG (final concentration) and grown for an additional 2 hours at 30°C. The cells were harvested by centrifugation and resuspended in 20 mL of resuspension buffer (buffer I; 1 M KCl, 5 mM $MgCl_2$, 1 mM β-mercaptoethanol, 50 mM Tris:HCl pH 8.0) supplemented with 0.1 mM PMSF, 1 mg/ml lysozyme and 1 U/mL of DNase I and incubated on ice for 30 min. After adding 10 mL of lysis buffer (buffer J; 500 mM KCl, 500 mM NaCl, 1% glycerol, 1 mM β-mercaptoethanol, 50 mM Tris:HCl pH 8.0), cells were lysed by one passage through a high-pressure cell disrupter (Stansted Fluid Power, 150 MPa), cell debris was removed by centrifugation (25,000 rpm for 40 min, JA-25.50 Beckman Coulter rotor) and clarified lysate was taken for protein purification.

Clarified cell lysate was filtered through a 0.2 μm syringe filter and loaded onto the HisTrap 1 mL HP column pre-equilibrated in buffer K (500 mM KCl, 500 mM NaCl, 10 mM $MgCl_2$, 1 mM β-mercaptoethanol, 0.002% mellitic acid, 15 mM imidazole, 50 mM Tris:HCl pH 8.0). The column was washed with 5 CV of buffer K, and the protein was eluted with a linear gradient (20 CV, 0%–100% buffer L) of buffer L (500 mM KCl, 500 mM NaCl, 10 mM $MgCl_2$, 1 mM β-mercaptoethanol, 0.002% mellitic acid, 500 mM imidazole, 50 mM Tris:HCl pH 8.0). Fractions most enriched in His_6-TEV-MESH1 (≈50%–60% buffer B) were pooled, totalling approximately 3 mL. The sample was loaded on a HiLoad 16/600 Superdex 200 pg column pre-equilibrated with buffer M (500 mM KCl, 500 mM NaCl, 10 mM $MgCl_2$, 1 mM β-mercaptoethanol, 0.002% mellitic acid, 50 mM Tris:HCl pH 8.0). The fractions containing His_6-TEV-MESH1 were pooled and subjected to buffer exchange by repeated filtration with an Amicon Ultra (Millipore) centrifugal filter device (cut-off 15 kDa) pre-equilibrated in buffer N (100 mM NaCl, 5 mM $MgCl_2$, 10% glycerol, 25 mM HEPES:KOH pH 7.5). The His-tag was cleaved off by adding TEV protease in a 1:100 molar ratio and the reaction mixture was incubated at 10°C for overnight. After the His6 tag was cleaved off, the protein was passed though 1 mL HisTrap HP pre-equilibrated with buffer N. Fractions containing MESH1 in the flow-through were collected and concentrated on Amicon Ultra (Millipore) centrifugal filter device with 15 kDa cut-off (final concentration is 4.75 μM). The purity of protein preparations was assessed by SDS-PAGE and spectrophotometrically (OD_{260}/OD_{280} ratio below 0.5). Protein preparations were aliquoted, frozen in liquid nitrogen and stored at –80°C.

C. marina ATfaRel (VHp313, pET24d-His6-aTfaRel) was overexpressed in freshly transformed *E. coli* BL21 DE3. Fresh transformants were inoculated to final OD_{600} of 0.05 in the LB medium (800 mL) supplemented with 100 μg/mL kanamycin. The cultures were grown at 37°C until an OD_{600} of 0.5, induced with 0.4 mM IPTG (final concentration) and grown for an additional one hour at 30°C. The cells were harvested by centrifugation and resuspended in 30 mL of binding buffer (buffer O; 2 M NaCl, 5 mM $MgCl_2$, 70 μM $MnCl_2$, 50 mM arginine, 50 mM glutamic acid, 1 mM Mellitic acid, 20 mM imidazole, 10% glycerol, 4 mM β-mercaptoethanol, 25 mM HEPES:KOH pH 7.6) supplemented with 0.1 mM PMSF and 1 U/mL of DNase I, and cells were lysed by one passage through a high-pressure cell disrupter (Stansted Fluid Power, 150 MPa), cell debris was removed by centrifugation (35,000 rpm for 45 min, Type 45 Ti Beckman Coulter rotor) and clarified lysate was taken for protein purification.

Clarified cell lysate was filtered through a 0.2 μm syringe filter and loaded onto the HisTrap 1 mL HP column pre-equilibrated in buffer O (2 M NaCl, 5 mM $MgCl_2$, 70 μM $MnCl_2$, 50 mM arginine, 50 mM glutamic acid, 1 mM Mellitic acid, 20 mM imidazole, 10% glycerol, 4 mM β-mercaptoethanol, 25 mM HEPES:KOH pH 7.6). The column was washed with 5 CV of buffer O, and the protein was eluted with a linear gradient (10 CV, 0%–100% buffer P) of buffer P (2 M NaCl, 5 mM $MgCl_2$, 70 μM $MnCl_2$, 50 mM arginine, 50 mM glutamic acid, 1 mM Mellitic acid, 500 mM imidazole, 4 mM β-mercaptoethanol, 25 mM HEPES:KOH pH 7.6). The fractions containing His_6-ATfaRel were pooled and subjected to buffer exchange by repeated filtration with an Amicon Ultra (Millipore) centrifugal filter device (cut-off 3 kDa) pre-equilibrated in buffer Q (500 mM KCl, 5 mM $MgCl_2$, 50 mM arginine, 50 mM glutamic acid, 10% glycerol, 4 mM β-mercaptoethanol, 25 mM HEPES:KOH pH 8.0). The purity of protein preparations was assessed by SDS-PAGE. Protein preparations were aliquoted, frozen in liquid nitrogen and stored at –80°C.

Preparation of *E. coli* fMet-$tRNA_i^{fMet}$ and $tRNA^{Phe}$ modified by Coprobacillus sp. D7 FaRel2

fMet-$tRNA_i^{fMet}$ was prepared as described in before (Murina et al., 2018) using non-radioactive methionine.

To modify $tRNA^{Phe}$, the reaction mixture containing 5 μM $tRNA^{Phe}$, 500 μM ATP and 50 nM FaRel2-$FLAG_3$ in HEPES:Polymix buffer, pH 7.5 (Takada et al., 2020) (5 mM Mg^{2+} final concentration) supplemented with 1 mM DTT was incubated at 37°C for 15 min. After that the reaction was supplemented with 0.1 volume of 3 M NaOAc (pH 4.6), the proteins were extracted with an equal volume of phenol/chloroform/isoamylalcohol (25:24:1), followed by a similar treatment with an equal volume of chloroform. As a negative control the same experiment was performed in the absence of FaRel2-$FLAG_3$. The extracted tRNA was mixed with 2.5 volume of 95% ethanol, precipitated at –20°C overnight and pelleted by centrifugation. The pellet was washed with 100 μL of ice-cold 70% ethanol, dried at room temperature for 5 minutes, and dissolved in 5 mM KOAc (pH 5.1). The concentration of the purified tRNA was calculated by measuring the absorbance at 260 nm, and phosphorylation was validated by aminoacylation reaction (see below).

Biochemical assays

Cell-free translation: experiments with PURExpress *In Vitro* Protein Synthesis Kit (NEB, E6800) were performed as per the manufacturer's instructions with the addition of 0.8 U/μL RNase Inhibitor Murine (NEB, M0314S). FaRel2-$FLAG_3$ was used at a final concentration of 50 nM, PhRel2-$FLAG_3$ at 100 nM and His_6-TEV-ATfaRel2 at 500 nM. As a control we used either HEPES:Polymix buffer, pH 7.5 (Takada et al., 2020) or eluate prepared from *E. coli* transformed with pBAD33 vector (mock). The total reaction volume was 6 μL per reaction for most of the experiments. To titrate the concentration of total tRNA in the reaction we used a combination of PURExpress Δ(aa, tRNA) Kit (NEB, E6840S) and total deacylated tRNA from *E. coli* MRE600 (Sigma-Aldrich, 10109541001). After incubation at 37°C for the indicated time, the reaction mixture was mixed with 9-fold volume of 2x sample buffer (100 mM Tris:HCl pH 6.8, 4% SDS, 0.02% bromophenol blue, 20% glycerol, 20 mM DTT and 4% β-mercaptoethanol), and 5 μL of the mixture was resolved on 18% SDS-PAGE gel. The SDS-PAGE gel was fixed by incubating for 5 min at room temperature in 50% ethanol solution supplemented with 2% phosphoric acid, then stained and detected as mentioned in protein expression and purification.

tRNA and oligonucleotide pyrophosphorylation by FaRel2 or PhRel2: the reaction conditions are described above, see 'Preparation of *E. coli* fMet-$tRNA_i^{fMet}$ and $tRNA^{Phe}$ modified by Coprobacillus sp. D7 FaRel2'. FaRel2-$FLAG_3$ was used at a final concentration of either 50 nM ($tRNA^{Phe}$ and $tRNA_i^{Met}$) or from 50 to 500 nM ($tRNA^{Val}$). PhRel2-$FLAG_3$ was used at a final concentration of 50 nM. Experiments with 5′-CACCN-3′ oligonucleotides used 50 μM oligonucleotides; tRNA (Chemical Block Ltd.) was used at a final

concentration of 5 μM. The total reaction volume was either 8 or 20 μL per reaction. The reactions were started by the addition of 500 μM γ^{32}P-ATP and incubated at 37°C for either 10 or 30 minutes. To calculate the ratio of phosphorylation, the reaction mixture was mixed in 10% trichloroacetic acid supplemented with 70 ng/μL *E. coli* total tRNA as co-precipitant, kept on ice for 30 minutes, and centrifuged at 21,000 g for 30 minutes at 4°C. After washing the pellet with 200 μL 10% TCA, tRNA was dissolved in 1 M Tris:HCl (pH 8.0) with shaking at 1,500 rpm for 20 min at 4°C. The radioactivity was quantified by scintillation counting in 5 mL of EcoLite Liquid Scintillation Cocktail (MP Biomedicals).

To visualize phosphorylated tRNA the reaction sample was mixed in 2 volumes of RNA dye (98% formamide, 10 mM EDTA, 0.3% bromophenol blue and 0.3% xylene cyanol), tRNA was denatured at 37°C for 10 min and resolved on urea-PAGE in 1 x TBE (8 M urea, 8% PAGE). The gel was stained with SYBR Gold (Life technologies, S11494) and exposed to an imaging plate overnight. The imaging plate was imaged by a Typhoon FLA 9500 (GE Healthcare). To visualize phosphorylated oligonucleotides the sample was resolved on urea-PAGE in 1 x TBE (5.6 M urea, 24% PAGE).

Effects of pyrophosphorylation by FaRel2 on tRNA aminoacylation: to probe the effect of FaRel2 on aminoacylation, 5 μM *E. coli* $tRNA^{Phe}$ (Chemical Block Ltd.) was pre-incubated at 37°C with or without 50 nM FaRel2 as well as in the presence or absence of 0.5 mM ATP for 10 minutes in HEPES:Polymix buffer, pH 7.5 (Takada et al., 2020) (5 mM Mg^{2+} final concentration) supplemented with 1 mM DTT and 160 μM ^{3}H-phenylalanine. The total reaction volume was 20 μL. The tRNA was then aminoacylated by adding the same volume of aminoacylation mixture (2 μM PheRS (40x excess over FaRel2) and 4 mM ATP in HEPES:Polymix buffer (5 mM Mg^{2+} final concentration), 1 mM DTT) followed by additional incubation at 37°C for 10 minutes. The reaction was quenched by adding trichloroacetic acid (TCA) to a final concentration of 10% as well as adding 70 ng/μL *E. coli* total tRNA as co-precipitant. After 30-minute incubation on ice, the tRNA was pelleted by centrifugation (21,000 g for 30 minutes at 4°C). The supernatant was discarded, the pellet washed with 10% TCA and the tRNA was dissolved in 1 M Tris:HCl (pH 8.0) with shaking at 1,500 rpm for 20 min at 4°C. Finally, ^{3}H-radioactivity was quantified by scintillation counting in 5 mL of EcoLite Liquid Scintillation Cocktail (MP Biomedicals).

In the case of experiments using SAH enzymes, 5 μM $tRNA^{Phe}$ with or without modification by FaRel2-$FLAG_3$ was pre-incubated for 10 minutes with or without 1 μM MESH1, His_6-ATfaRel or His_6-TEV-ATfaRel2 at 37°C in HEPES:Polymix buffer pH 7.5 (5 mM Mg^{2+} final concentration) (Takada et al., 2020) additionally supplemented with 1 mM $MnCl_2$, 160 μM ^{3}H-phenylalanine and 1 mM DTT. After 10 minute PheRS was added to final concentration of 1 μM and after additional 10 minutes at 37°C the reaction was quenched by TCA and incorporation of the ^{3}H-radioactivity was quantified by scintillation counting (see above).

^{3}H-ppGpp synthesis by E. coli RelA: E. coli RelA synthase activity assay was performed in HEPES:Polymix buffer (5 mM Mg^{2+} final concentration) as described earlier (Takada et al., 2020) with minor modifications. Specifically, the assay was performed in the presence of 300 μM ^{3}H-GDP, 1 mM ATP, 100 μM pppGpp, 50 nM native RelA and 100 nM 70S IC(MVF), in the presence or absence of 100 nM *E. coli* deacylated $tRNA^{Val}$ (Chemical Block Ltd.); 5 μL total reaction volume per time point. *E. coli* deacylated $tRNA^{Val}$ and ATP were initially incubated with either HEPES:Polymix buffer, empty vector lysate, or lysate containing FaRel2, at 37°C for 30 minutes. GDP, pppGpp, and 70S IC were then added and the reactions were started by the addition of RelA. Subsequently, aliquots were withdrawn from the reaction mix, resolved on PEI-TLC, radioactivity quantified by scintillation counting and the turnovers were determined as previously described (Turnbull et al., 2019).

Mass spectrometry

E. coli $tRNA^{Phe}$ was pyrophosphorylated by FaRel2 as described above, then desalted by Centri-Sep (Thermo Fisher Scientific) to remove ATP. The tRNA (2 pmol) treated or untreated with FaRel2 was digested with RNase T_1 (10U, Thermo Fisher Scientific) in 25 mM ammonium acetate (pH 5.3) at 37°C for 45 min. The digests were mixed with one-tenth volume of 0.1 M triethylamine acetate (pH 7.0), and then subjected to capillary LC/nano ESI-MS on an Q Exactive Orbitrap mass spectrometer (Thermo Fisher Scientific) equipped with a splitless nanoflow HPLC system (DiNa, Techno Alpha Co. Ltd) using a trap column (L-column2, ODS, 5um, 0.3 × 5 mm, Chemicals Evaluation and Research Institute) and a capillary column (HiQ Sil C18W-3, 0.1 × 100 mm, Techno Alpha Co. Ltd) (Akichika et al., 2019; Suzuki et al., 2007; Suzuki et al., 2020). Composition of solvent A is 0.4 M 1,1,1,3,3,3-Hexafluoro-2-propanol (HFIP, adjusted to pH 7.0 with triethylamine), and solvent B is 0.4 M HFIP (pH 7.0) / 50% MeOH. The digested tRNA fragments were separated using a linear gradient of 5 to 100%B in 35 min at 300 nL/min. The eluent was ionized by an ESI source in negative polarity mode and scanned over an *m/z* range from 600 to 2000. The target ions were fragmented in the Higher-Energy Collision Dissociation (HCD) cell with stepped normalized collision energy of 20, 25 and 30%.

Structural modeling and docking

The structure of FaRel2 was modeled using Rosetta (Song et al., 2013) based on the coordinates of *S. aureus* RelP (Manav et al., 2018) and *B. subtilis* RelQ (Steinchen et al., 2015). The models with the best scores were used for molecular docking as implemented in the web server version of HADDOCK (High ambiguity driven biomolecular docking) (van Zundert et al., 2016) together with the coordinates of yeast $tRNA^{Phe}$ (Nissen et al., 1995).

For the docking procedure we defined residues in the active site; Y128 and the catalytic glutamine were selected as active residues (i.e., directly involved in the interaction). We then allowed HADDOCK to automatically select passive residues around the active residues. The program was run with default settings. The best cluster resulting from the docking experiment was selected to further probe the catalytic mechanism of FaRel2.

Figure preparation

Figures were prepared using UCSF ChimeraX (Goddard et al., 2018), Igor Pro (WaveMetrics, Inc.), Adobe Illustrator (Adobe Inc.) and Adobe Photoshop (Adobe Inc.).

QUANTIFICATION AND STATISTICAL ANALYSIS

Statistical analysis of tRNA aminoacylation, tRNA pyrophosphorylation and ^{3}H-ppGpp synthesis data was performed using Igor Pro (WaveMetrics, Inc.). The data was plotted as individual data points as well as mean values ± standard deviations.